Ph.D. degree in Systems Medicine

Curriculum in Human Genetics, XXXIV Cycle, Area MED/03

European School of Molecular Medicine (SEMM), Naples site

University of Milan and University of Naples “Federico II”

Liver fibrosis impairs hepatocyte transduction by AAV vectors

Gemma Bruno

Telethon Institute of Genetic and Medicine (TIGEM), Naples, Italy

Student number R12432

Tutor: Dr. Pasquale Piccolo

Telethon Institute of Genetic and Medicine (TIGEM), Naples, Italy

Internal Supervisor: Prof. Alberto Auricchio

Dept. of Advanced Biomedicine, “Federico II” University, Naples, Italy

Telethon Institute of Genetic and Medicine (TIGEM), Naples, Italy

External Supervisor: Prof. Leszek Lisowski

Faculty of Medicine and Health, University of Sidney, Australia

Children’s Medical Research Institute (CMRI), Westmead, Australia

Academic year 2021-2022

TABLE OF CONTENTS

LIST OF ABBREVIATIONS

AAP	assembly activating protein
AAV	adeno-associated vector
AAV8	AAV serotype 8
AAVR	AAV receptor
AUC	area under the curve
CMV	cytomegalovirus
CCl_4	carbon tetrachloride
dsDNA	double-stranded DNA
ECM	extracellular matrix
eGFP	enhanced green fluorescent protein
gc	genome copies
HCC	hepatocellular carcinoma
HSC	hepatic stellate cells
ITRs	inverted terminal repeats
i.v.	intravenously
KC	Kupffer cells
LamR	37/67-kDa laminin receptor
LNP	lipid nanoparticle
NHPs	non-human primates
ORF	open reading frame
pA	poly(A)
PCR	polymerase chain reaction
PFA	paraformaldehyde
PFIC3	progressive familial intrahepatic cholestasis type 3
rAAV	recombinant adeno-associated vector
SEC	sinusoidal endothelial cells
SEM	standard error of mean
ssDNA	single-stranded DNA
TAA	thioacetamide
TBG	thyroxine-binding globulin
VP1, VP2, VP3	virion protein 1, virion protein 2, virion protein 3
WD	Wilson disease

LIST OF FIGURES

ABSTRACT

Adeno-associated viral vectors (AAVs) are the most promising tools for liver-directed gene therapy. However, integrity of hepatic architecture has been considered pre-requisite for efficient gene delivery and clinical studies have been addressed toward patients with no or negligible hepatic damage and fibrosis. Preliminary evidence suggests that AAV-mediated gene transfer to hepatocytes may be hampered by liver fibrosis, but knowledge about AAV vector interactions with fibrotic livers is still very limited. In the present study, we investigated hepatocyte transduction and biodistribution of AAV8-based vectors, commonly used in liver-directed gene therapy clinical trials, in the context of liver fibrosis.

Analysis of three mouse models of induced and genetic liver fibrosis revealed that fibrotic livers are transduced less efficiently by AAV8 and this results from reduced vector uptake by the liver. Moreover, liver fibrosis altered blood vector clearance and vector biodistribution in extra-hepatic organs.

Overall, these findings demonstrated that liver fibrosis impairs AAV-mediated gene transfer to hepatocytes and highlight the relevance of the limitations posed by liver fibrosis to efficient and safe gene transfer.

INTRODUCTION

1. Gene therapy

Gene therapy is a medical approach aimed at replacing, manipulating or supplementing nonfunctional or malfunctional genes with healthy ones to treat monogenic diseases [1]. The therapeutic gene is administered to patients through a vector promoting transgene delivery into patients' cells.

There are two types of gene therapy: *in vivo* and *ex vivo* [1]. The in *vivo* gene therapy is based on the administration of the vector containing the therapeutic gene directly into the blood circulation to reach target organs. The ex *vivo* gene therapy consists in the isolation and manipulation of target cells from patient, that are then infused back to the patient. This thesis is focused on liver-directed *in vivo* gene therapy.

1.1 Gene therapy vectors

An ideal gene therapy delivery system should meet all of the following criteria:

- cargo capacity to accommodate gene of interest
- protection of genetic cargo from degradation
- efficient delivery of genetic material to target cells
- favorable safety profile
- economical and feasible for patients

For this purpose, choice of the proper gene therapy vector to targeted cells should carefully evaluated.

Several *in vivo* delivery systems have been described so far, including non-viral and viral vectors. Briefly, both delivery platforms differ on type of vectors, stability, transduction efficacy, expression of transgene, immunogenicity and costs of production [2]. The first, mostly represented by lipid nanoparticles (LNP) and cationic polymers, exhibit advantages such as being less cost-effective and having a good safety profile, but their transduction efficiency and specificity is low [2]. Viral vectors, instead, are derived from natural viruses that were engineered to be safely used for clinical application [2].

1.2 Adeno-associated viral vectors

Adeno-associated viral vectors (AAVs) have emerged as vector of choice for in vivo gene therapy in preclinical studies and clinical trials [3]. AAVs is a ~4.7kb single strand DNA (ssDNA) virus belonging to the Parvoviridae family [4]. Its genome includes *rep*

and *cap* gene flanked by two T-shaped inverted terminal repeats (ITRs). The *rep* gene encodes four proteins (Rep78, Rep68, Rep52 and Rep40) known to be crucial for genome replication and virion assembly [4]. The *cap* gene encodes three capsid proteins (VP1, VP2 and VP3) starting from a single open reading frame (ORF) and regulated by alternative splicing [4]. A third gene, encoding the assembly activating protein (AAP), is encoded within the *cap* gene and promotes virion assembly [5] (Fig. 1). Recently, the membrane-associated accessory protein (MAAP) has been identified in the *cap* region and demonstrated its ability to promote AAV replication and to control adenoviral infection [6].

AAVs have a non-enveloped icosahedral protein capsid of ~26nm consisting of 60 subunits of VP1: VP2: VP3 in a ratio of 1: 1: 10. Nine variable regions on AAV capsid surface have been reported so far, these surface topologies are responsible for tissue tropism as well as AAV intracellular trafficking and are recognized by neutralizing antibodies (NAbs) [7; 8].

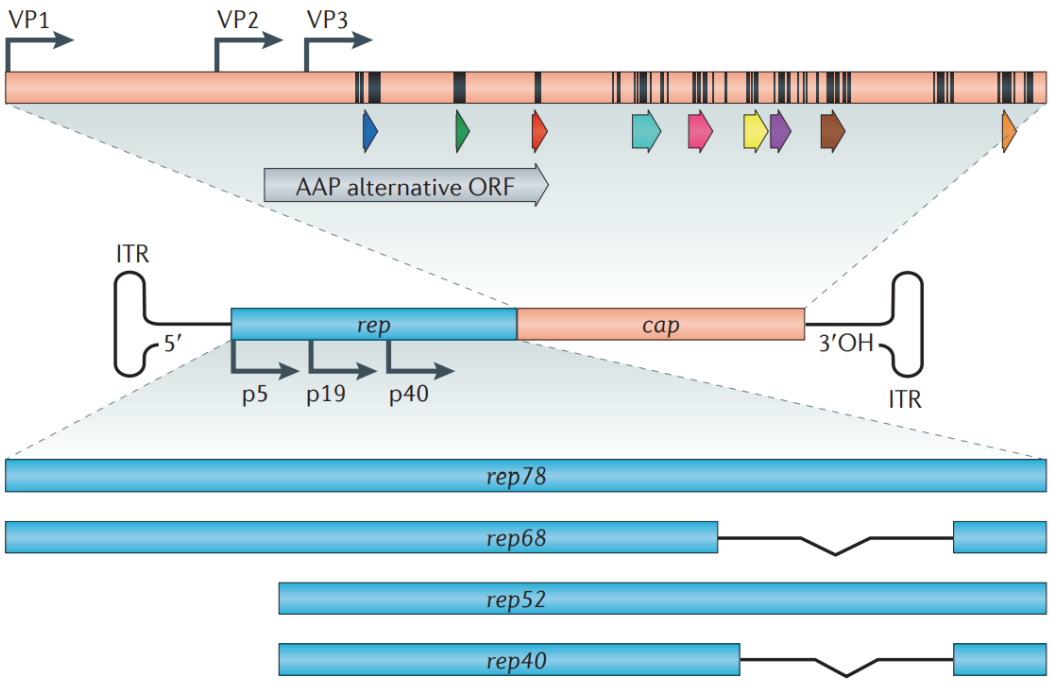

Figure 1: Genome of adeno-associated vectors

The 4.7kb ssDNA of genome of AAV is reported. The AAV genome is packaged in a non-enveloped icosahedral capsid containing *rep* (indicated in light blue), *cap* (indicated in pink) and AAP (indicated in grey within the *cap* gene) flanked by ITRs (T-shape indicated in black). Hypervariable regions are shown as colored arrows. Regions encoding surface-exposed amino acids are indicated as black lines on *cap* genes. Adapted from [9].

ITRs are 145 bp long and are necessary for viral genome replication and packaging. Recombinant AAV (rAAVs) undergo manipulation in order to replace viral genes

with a DNA of interest [10]. During production steps, *rep* and *cap* are provided in trans by a packaging plasmid together with adenoviral helper genes, known to be essential for replication [11].Thus, the gene of interest is inserted between the ITRs which are the only *cis* elements needed to generate rAAV particles.

1.3 AAV biology

To date several natural serotypes have been identified, hundreds of variants isolated and several others have been generated by vector engineering to improve AAV-mediated gene delivery [9].

AAV-mediated gene transfer efficiency depends on AAV entry, that is determined by the binding of capsid proteins with receptor and co-receptors of surface of target cells [12] (Fig. 2). Each serotype is able to recognize distinct cell receptors thus exhibiting tissue- and cell-specific tropism [10]. AAV binding to surface receptors triggers viral particle internalization through endosome-mediated endocytosis [13]. Trapped into the endosomal compartment, AAVs traffic through the cytosol via cytoskeleton components [14] and undergo pH-dependent structural rearrangement crucial for transduction [15] (Fig. 2). After endosomal escape, AAVs reach the nucleus through the nuclear pore complex, capsid is disassembled and its genome is released [16]. Intracellular trafficking consists of multiple processes that can unsuccess in some steps resulting in incomplete gene delivery and AAV degradation (Fig. 2). At nuclear level, AAV ssDNA is converted to double-stranded DNA (dsDNA) [17], transcribed to mRNA and exported to cytosol for translation. ITRs can trigger inter- and intra-molecular recombination of circularized non replicating episomal genomes that can persist in the nucleus, leading to gene expression in post-mitotic cells [18]. Importantly, integration events within the host DNA are occurring even if AAV genome is devoid of *rep* gene. Integration has been identified to occur preferentially into the murine *Rian* genomic locus [19], thus highlighting risk of insertional mutagenesis related to AAV administration. Moreover, integration events may interest portion of the AAV genome occurring, even if at low rates, in an unsupervised manner and not desirable for therapeutic purposes.

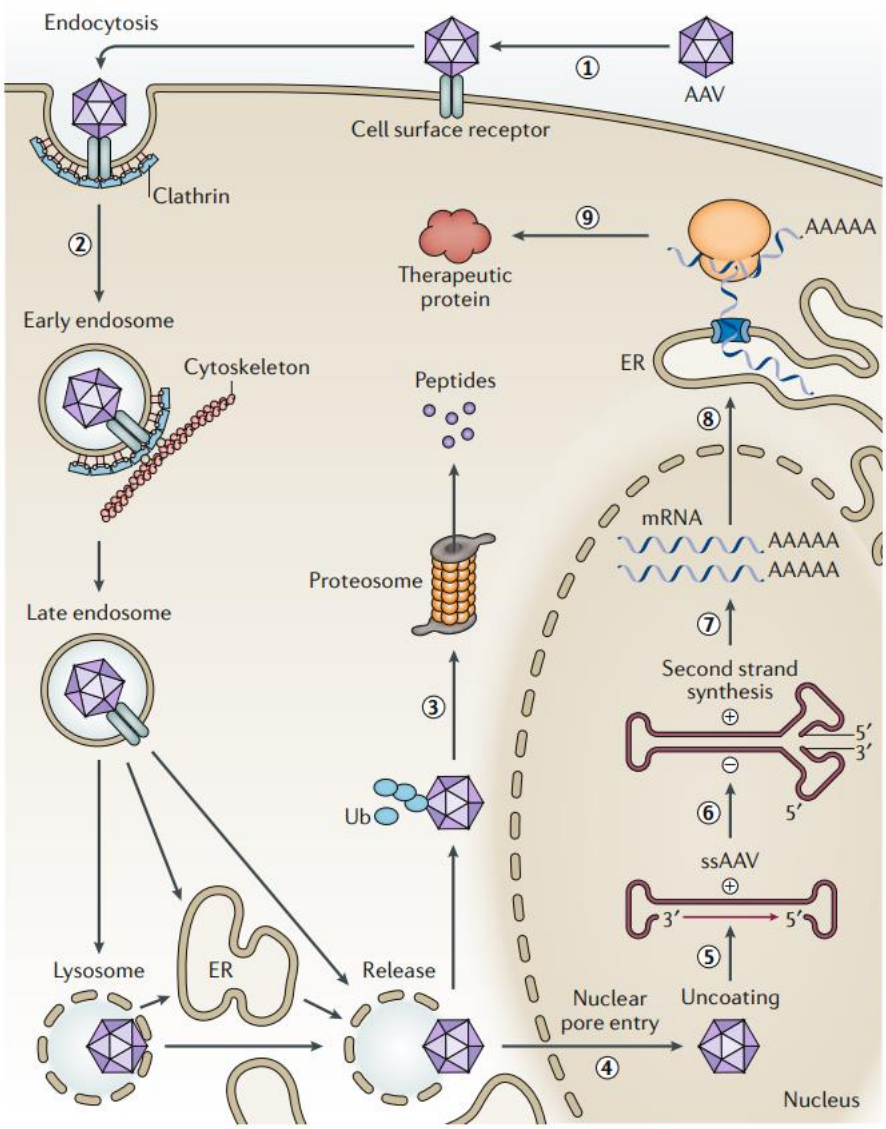

Figure 2: AAV vectors internalization, intracellular trafficking and transduction pathway

(1) AAV binds to receptor and co-receptor on surface of targeted cells. (2) AAV internalization is mediated through endosome-mediated endocytosis and traffic to the cytosol is dependent on cytoskeleton. (3) pH-dependent structural changes promote endosomal escape, ubiquitylation (Ub) and subsequent proteasome degradation can occur. (4) AAV traffics to the nucleus, (5) uncoating of virions occurs and AAV genome is released. (6) ssDNA is converted to dsDNA, (7) dsDNA is transcribed into mRNA and (8) exported to the cytosol for translation and expression of the therapeutic protein (9). Adapted from [4].

2. The liver

The liver is one of the largest organs in the body where it orchestrates a huge variety of functions including metabolism of nutrients, degradation of toxic compounds, immunologic functions, synthesis of circulating proteins and storage of substances.

2.1 Liver structure

The liver receives approximately 25% of the cardiac output with a dual blood supply [20]: 75% is provided from portal vein while the remaining 25% from the hepatic artery [20, 21]. Portal blood originates from gastrointestinal tract while the hepatic artery branches from celiac trunk and descending aorta. The portal vein divides repeatedly into smaller venules that finally drains into the sinusoids, the hepatic artery forms arterioles and capillaries into liver sinusoids too [21]. Both blood sources meets at the liver sinusoids as a final destination, that is considered a specialized capillaries network where exchange of nutrients occurs between perisinusoidal space and the sinusoids [21]. Once filtered through sinusoids blood flow tills the central vein where it leaves the liver through the hepatic vein [21] (Fig. 3).

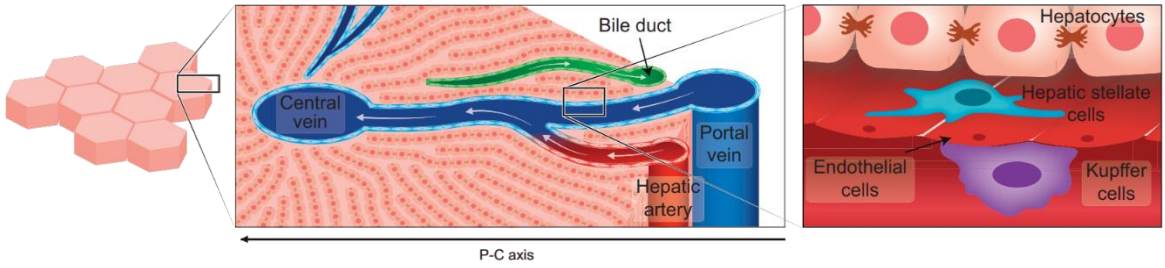

Figure 3: Liver lobule structure and hepatic cell types

Basolateral membranes of hepatocytes are decorated with microvilli and are in contact with perisinusoidal space allowing for nutrients and molecules sequestration. SECs delimitate hepatic sinusoids that are dispersed with KCs. HSCs are localized within the perisinusoidal space. Adapted from [22].

The functional unit of the liver is the lobule, characterized by a typical hexagonal shape [20] hosting the central vein at its center [23] (Fig. 3). Hepatocytes, representing the 60% of hepatic cell type and performing the majority of the hepatic functions, radiate from the central vein to the edge of the lobule [23]. The space between radiating hepatocytes is represented by sinusoids, canals of 8-10µm, lined with endothelial cells (SEC) and hosting Kupffer cells (KC), hepatic resident macrophages and are dispersed within the sinusoids allowing for pathogens removal and phagocytic activity [21; 23; 24].

SECs are devoid of basement membrane to promote exchange of nutrients and molecules between perisinusoidal space and blood [21]. Substances can diffuse through the fenestrations of sinusoids (approximately 100nm in diameter) into the space of Disse and be taken up by hepatocytes [25]. Hepatic stellate cells (HSC) are localized in the perisinusoidal space and contain lipid droplets enriched with vitamin

A [24]. HSCs are activated by stressful conditions and differentiate into myofibroblast-like cells deposing huge amounts of extracellular matrix (ECM) components in the perisinusoidal space in response to chronic liver injuries [21]. Thanks to its size of approximately 25nm [25], blood-borne AAV can cross fenestrations of hepatic sinusoids and easily access space of Disse and infect hepatocytes [25].

2.2 Liver fibrosis

Liver fibrosis is a pathological condition that arises in response to chronic hepatic insults and is characterized by abnormal deposition of ECM components in the hepatic parenchyma [23]. Alcohol and drug abuse, viral hepatitis, genetic disorders and cholestatic diseases represent some of the causes responsible for liver fibrosis. If chronic injury persists, liver fibrosis can progress to cirrhosis which is characterized by altered organ architecture, aberrant vasculature and multiple regenerative nodules resulting in portal hypertension, hepatocellular carcinoma (HCC) and organ failure [26].

Various biological and physical changes occur during fibrosis development and progression:

i. immune cells infiltration to promote tissue repair [23] and inflammatory cytokines secretion [26];
ii. deposition of fibrogenic type I and III collagens within the perisinusoidal space resulting in disruption of radial arrangement of hepatocytes [23; 26];
iii. accumulation of ECM also conferring a mechanical rigidity to the liver and leading to intrahepatic vasoconstriction, vascular resistance and portal hypertension [23];
iv. loss of sinusoidal fenestration and hepatocytes microvilli, thus hampering exchange of nutrients and molecules [23].

Noteworthy, until decompensated cirrhotic stage is reached, liver fibrosis could be reverted if the insult is removed [26].

2.3 Models of liver fibrosis

Numerous models of liver fibrosis have been described so far [27]. In the present thesis, we focused on acquired (hepatotoxin-induced models) and genetic models of liver fibrosis, that are characterized by a different fibrosis pattern and progression and are representative of the fibrosis scenarios occurring in humans.

Thioacetamide (TAA) is a well-known inducer of liver damage and fibrosis. TAA is a thiono-sulfur compound metabolized by hepatocytes in S- and S-S bioactive

oxides, intermediates responsible for hepatotoxicity induction, and result in pericentral fibrosis, that progresses to pan-lobular fibrosis at later stages [27].

Several genetic disorders are characterized by liver fibrosis, including familiar forms of cholestasis, Wilson disease and α-1 antitrypsin deficiency [28]. The *Atp7b*$^{-/-}$ mouse [29] recapitulates several features of the Wilson disease (WD), an autosomal recessive disorder of copper metabolism. In this mouse excessive hepatic copper storage starts in the first weeks of life and liver develops steatosis and mild inflammation by six weeks of age, progressing into hepatitis, necroinflammation and extensive perisinusoidal fibrosis by the age of eighteen to twenty weeks [30].

The *Abcb4*$^{-/-}$ mouse is a widely used model of biliary fibrosis and resembles clinical features of progressive familial intrahepatic cholestasis type 3 (PFIC3) and primary sclerosing cholangitis [31; 32]. ABCB4-deficiency results in toxic bile acid accumulation in hepatocytes and bile, triggering profibrogenic cholangiocyte response. *Abcb4*$^{-/-}$ mice develop moderate fibrosis by three weeks of age and severe portal fibrosis with ductular reaction by ten-twelve weeks of age [33].

3. Liver directed gene therapy

The liver represents an attractive organ for gene therapy of genetic disorders due to deficiency of enzymes operating in hepatocytes or diseases that can be ameliorated by proteins produced and secreted by hepatocytes [25]. Moreover, several non-viral and viral vectors can achieve efficient gene transfer to hepatocytes [34]. AAV are currently the vector of choice and two AAV-based products for the treatment of hemophilia A and B have recently achieved market authorization [35; 36]. Dozens of clinical trials are currently in the pipeline for liver indications, employing both natural and engineered AAV variants [34].

3.1 Natural AAV serotypes for liver directed gene therapy

Natural AAV serotypes have been isolated from human and non-human primates (NHPs) and are classified in clades based on their sequence homology and seroreactivity [37]. So far, 13 serotypes have been described, while hundreds of viral isolates have been retrieved from mammals and other animal species [38].

Previous works evaluated ability of natural serotypes to transduce the liver: AAV5, AAV8 and AAV9 being the most common variant used in clinical trials for liver-directed gene therapy [4; 25; 34; 39]. Nevertheless, recently the AAV3B was found to be more efficient in transduction of both NHP and human hepatocytes in humanized mouse models [40; 41; 42].

Each serotype can interact with specific receptor and co-receptor to promote intracellular uptake of the virus. To date, different receptor and co-receptor responsible for surface interaction in targeted tissue of AAV serotypes have been identified so far [43]. AAV8 primary receptor(s) responsible for surface recognition in host cells are still unknown while AAV receptor (AAVR) [4] and the 37/67-kDa laminin receptor (LamR) [4], [44] have been associated as co-receptor for this serotype.

3.2 Engineered AAV variants

Engineering AAV capsids have acquired lot of interest in the last decade. Novel capsid development can account on four different approaches: natural discovery, rational design, directed evolution and in silico design [10] (Fig. 4).

Natural discovery is based on isolation of novel AAV variants from human and non-human sources. Noteworthy, most of the vectors that reached clinical stage have been isolated from natural sources, in particular from primates. Variants isolated from other vertebrates have the lowest theoretical chance of being recognized by pre-existing NAbs in patients [10], but they may also exhibit lower transduction efficiency in humans.

Rational design of capsid modifications consists of targeted crafting of capsid peptide sequence to influence specific interactions with cell receptors or antibodies [45]. To this aim, specific peptide sequences or variable fragments are introduced on capsid surface to improve cell- or tissue-specific receptor binding [10]. However, knowledge about the interaction of the AAV capsid with target cells is needed. Moreover, peptide insertion can also occur on the 3-fold protrusion of the capsid which are known to be tolerant to modification, influence tissue tropism and modulate immunogenicity of the capsid [10]. This was the case for AAVS3, tested in clinical trials to treat Hemophilia B [46] and Fabry disease [47], that was rationally designed to improve hepatic transduction by merging VP1 region from AAV8 with VP2 and VP3 from AAV3B capsid [48].

In silico design consists of computational tools to design AAV capsid without needing of capsid biology knowledge [10]. High-throughput sequencing and bioinformatic tools can be used to design combinatorial capsid variants by virtually modifying variable regions on the surface of the capsid [49]. Moreover, *in silico* phylogenetic and statistical tools can promote identification of intermediate or ancestral serotypes. Anc80, predicted ancestor of AAV1, AAV2, AAV8, and AAV9, was identified as gene therapy vector to target liver, muscle and retina [50] by *in silico* design.

Directed evolution mimics natural evolution by applying a selective pressure (e.g. the ability to infect a specific cell type) to promote the emergence of genetic variants that confer specific biological properties to the AAV capsid [10]. The process involves the generation of large genetic libraries of *cap* genes, encoding for capsid proteins, by fragmentation and reassembly (shuffling) of *cap* sequences from existing AAV serotypes or by random mutagenesis by error-prone PCR. AAV libraries undergo rounds of in vivo selection. Directed evolution has been successfully employed to generate novel AAV variants for liver-directed gene therapy: AAV-DJ resulted from the evolution of natural occurring AAVs in human hepatocytes incubated with human immunoglobulins, to confer NAb-evasion properties [51], while AAV-LK03 was developed by directed evolution in mouse models with human hepatocyte xenografts [52] and is currently under clinical investigation for hemophilia A (NCT03734588, NCT03003533) and methylmalonic acidemia (NCT04581785).

Taken together these approaches can contribute to design and identification of AAV capsid variants with desired properties aimed at increasing transduction efficiency in targeted cells or tissues and reducing AAV immune interactions.

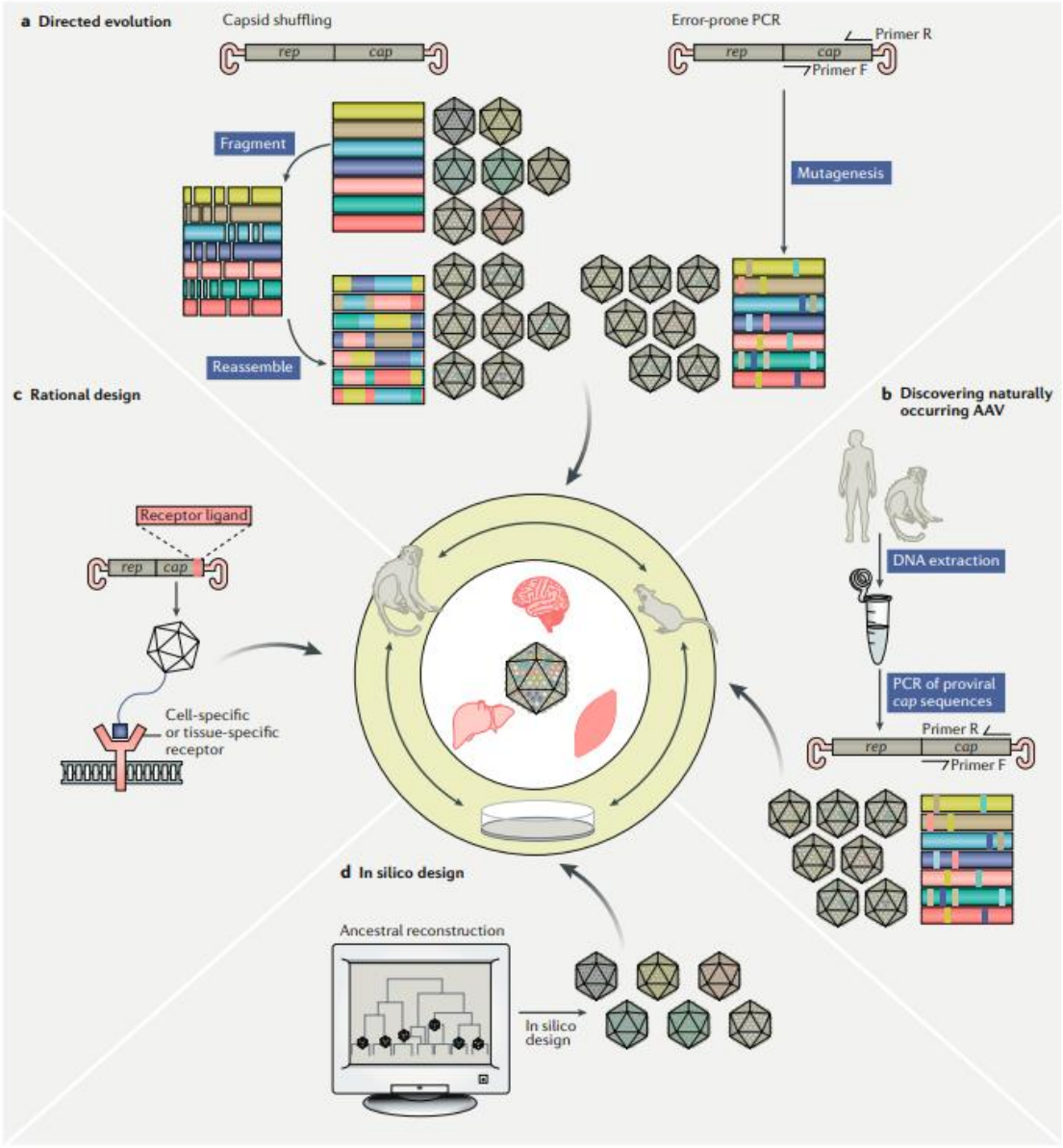

Figure 4: Methods for capsid discovery and engineering

(A) Directed evolution is based on capsid shuffling and error-prone PCR to generate novel capsid variants. (B) Natural occurring AAVs are isolated from human and non-human sources. (C) Rational design is based on knowledge on capsid biology as well as host cell targets to specifically recognize cell- or tissue- receptor and evade immune recognition. (D) *In silico* design consists of computational approaches to predict capsid variants not identified in nature. Adapted from [10].

3.4 AAV Gene therapy in the context of liver fibrosis

Intact hepatic architecture has been so far considered a prerequisite for efficient gene transfer using AAVs and patients presenting clinically relevant liver fibrosis are currently excluded from clinical trials. Indeed, fibrosis development and progression result in several biological and physical changes that may affect liver-directed gene therapy efficacy and safety:

i. deposition of extracellular matrix in the perisinusoidal space and loss of sinusoid fenestrations, that reduce vascular permeability and may hamper the contact of blood-borne vectors with hepatocytes [53];
ii. infiltration and proliferation of immune cells, that may result in enhanced vector scavenging and immune reaction toward the vector [54; 55];
iii. inflammation associated to fibrosis, which may contribute to priming of immune cells [56];
iv. regenerative response to hepatocellular damage, resulting in increased hepatocyte proliferation and rapid episomal vector dilution [57].

Taken together modification altering hepatic architecture occurring in presence of liver fibrosis are expected to influence AAV-mediated hepatic transduction.

To date, very few studies have investigated the delivery of AAV vectors in animal models of fibrotic liver diseases, while no data are available from human studies. Adenoviral vectors have been previously reported to show a reduced transduction efficiency in cirrhotic rat livers, suggesting that distorted liver architecture affected hepatocytes transduction [58]. Another study demonstrated AAV1 administration in cirrhotic versus non cirrhotic rats showed similar hepatocyte transduction levels [59]. It should be noted that AAV1 is not an hepatotropic serotype [39] and it is able to transduce mouse hepatocytes at low levels [60]. AAV8 vectors administered in *Abcb4*$^{-/-}$ mouse exhibited a remarkable reduction in transgene expression if injected after liver fibrosis development [61]. Moreover, AAV8 administered to *Atp7b*$^{-/-}$ mouse failed to reach therapeutic efficacy in presence of established hepatic fibrosis [62]. Liver fibrosis might represent a physical barrier to AAV vectors delivery to hepatocytes as well as alter AAV tropism to its specific targets. This is the case for AAV2 that showed tropism for hepatic stellate cells in carbon tetrachloride-induced liver fibrosis [63]. Taken together, these findings suggest that liver fibrosis hampers hepatocyte transduction and its effect may be dependent on AAV serotype. The present thesis highlights the importance of a deeper investigation and characterization of how liver fibrosis influences AAV-mediated hepatic transduction.

AIMS OF THE THESIS

The overall objective of this thesis was to investigate the effect of fibrosis on liver-directed gene therapy mediated by AAV vectors.

The first aim was to evaluate effect of liver fibrosis on AAV vector transduction efficiency. To this aim, AAV2/8 particles packaging an enhanced green fluorescent protein (eGFP) under the control of thyroxine-binding globulin (TBG) were administered to animal models with liver fibrosis. I investigated AAV vector biodistribution and transduction of hepatocytes in different mouse models with liver fibrosis.

The second aim was to develop novel synthetic AAVs to efficiently transduce hepatocyte in genetic diseases with liver fibrosis. We generated a library of chimeric AAV capsids and will select the best at infecting hepatocytes in mouse models of liver genetic disorders with fibrosis using directed evolution approach.

MATERIALS AND METHODS

Plasmids

Plasmids used for AAV vector production were AAV2/8 indicating the virus is containing genome of serotype 2 packaged into capsid from serotype 8. eGFP was subcloned into pAAV2/8 under the control of TBG promoter for *in vivo* studies. Expression cassettes also included Simian virus 40 (SV40) intron, woodchuck hepatitis virus post-transcriptional regulatory element (WPRE), and bovine growth hormone polyadenylation signal (bGHpA).

AAV vector production

AAV2/8 vectors were produced by InnovaVector (Pozzuoli, Italy) by triple transfection of HEK293 cells with (i) TBG.eGFP; (ii) pTigem Helper, which supplies the adenoviral genes for replication; and (iii) pTigem Rep/Cap, which contains the gene sequence for the replication protein (*rep*) of AAV2 and for the capsid (*cap*) proteins of the selected serotype. AAV2/8 vectors were then purified by two rounds of $CsCl_2$ gradients. Physical titers of the viral preparations (genome copies per milliliter) were determined by real-time PCR quantification using TaqMan (Applied Biosystems) and dot-blot analysis. The final titer of each preparation was calculated as the average between the PCR quantification and dot-blot results.

Animal procedures

Mouse procedures were carried out in accordance with the regulations and authorized by the Italian Ministry of Health. C57BL/6 wild-type mice (Charles River Laboratories), *Atp7b*$^{-/-}$ and *Abcb4*$^{-/-}$ mice were housed under specific pathogen-free condition at TIGEM animal facility (Pozzuoli, Italy) with 12-hour light/dark cycles and received food and water provided *ab libitum*. *Atp7b*$^{-/-}$ and C57BL/6 male mice were used for experimental procedures, while for studies in *Abcb4*$^{-/-}$ mice both male and female mice were employed. C57BL/6 wild-type mice were administered with increasing doses of TAA or vehicle (PBS) as previously reported [27] for 12 weeks and then intravenously (i.v.) injected with an AAV8 vector encoding GFP under the control of TBG promoter (AAV2/8.TBG.eGFP) at the dose of $1X10^{13}$ gc/Kg. C57BL/6 wild-type mice were sacrificed 4 weeks post-AAV injection. *Atp7b*$^{-/-}$ and *Abcb4*$^{-/-}$ mice were injected with an AAV8 vector encoding GFP under the control of TBG promoter (AAV2/8.TBG.eGFP) at the dose of $5X10^{12}$ gc/Kg and harvested 2 days

and 14 days post-injection. Blood samples were collected from all the animal models at 0-, 1-, 3-, 6- and 24-hours post-injection. At sacrifice, animals were perfused with PBS and livers were harvested for further analysis.

Blood collection and analysis

Blood was collected by tail bleeding and placed in lithium heparin–coated vessels. Serum was separated by centrifugation and stored at −20°C prior to analyses. Genomic DNA was purified using NucleoSpin® Blood according to manufacturer's protocol (Macherey-Nagel) and evaluated by real-time PCR targeting the TBG sequence, using the Quantitect Sybr Green Kit (Qiagen, Germantown, MD). Standard curves were generated using serial dilutions of linearized plasmid containing TBG eGFP.

Vector copy number analysis

Using standard phenol-chloroform and ethanol precipitation methods genomic DNA was extracted from 30-50 mg of snap-frozen liver, spleen, kidney, lung, brain, bone marrow and heart. Briefly, total DNA was isolated from liver tissues with Hirt solution (10mM Tris, 10mM EDTA pH 7.5, and 0.6% SDS) supplemented with 20 µg/µL overnight at 55°C under movement. 100 µg/µL of RNAse A were added to the mixture and incubated for one hour at 37°C. DNA was recovered after two rounds of phenol-chloroform and over-night precipitated in ethanol supplemented with 3M sodium acetate. Pelleted DNA was centrifuged at maximum speed for 60' at 4°C, washed twice with 70% ethanol, dried at 55°C and resuspended in MQ H2O.

Vector copy numbers were determined by quantitative real-time PCR targeting the TBG sequence, using the Quantitect Sybr Green Kit (Qiagen, Germantown, MD). Standard curves were generated using serial dilutions of linearized plasmid containing TBG eGFP.

Histology and immunofluorescence

Livers from PBS-perfused mice were fixed in 4% paraformaldehyde for 12 h, stored in 70% ethanol, and embedded in paraffin blocks.

For Sirius red staining, 5-µm-thick sections were rehydrated and stained for 1 h in picrosirius red solution (0.1% Sirius red in saturated aqueous solution of picric acid). After two changes of acidified water (0.5% acetic acid in water), sections were dehydrated, cleared in Sub-X, and mounted in a resinous medium.

Livers from PBS-perfused mice were fixed in 4% paraformaldehyde for 12 h, cryopreserved in 10%-30% (wt/vol) sucrose, frozen in optimal cutting temperature compound (Tissue-Tek O.C.T.; Kaltek) in OCT blocks.

For immunofluorescence staining eGFP expression was evaluated on 5 µm frozen sections were permeabilized with 0.2% Triton X with 75mM NH_4Cl in PBS for 30' at room temperature. Sections were washed twice in PBS and blocked for 60' at room temperature with 5% donkey serum, 3% BSA, 20mM $MgCl_2$, 0,3% Triton X in PBS. First antibody was incubated overnight at 4°C using chicken GFP (Abcam, Cat#13970). The day after, sections were washed twice with 0,2% Triton X in PBS and incubated for 60' at room temperature with donkey anti-chicken Alexafluor 488 (Invitrogen, Cat# A78948) and DAPI (Invitrogen, Cat#1306). Sections were washed twice with 0,2% Triton X in PBS and mounted with mowiol mounting medium.

Images were captured by Axio Scan.Z1 microscope (Zeiss) and analyzed using ImageJ software for quantification of Sirius red positive and GFP positive areas. At least five images for each mouse were analyzed.

Western blot analysis

30 mg of snap-frozen livers were lysed in RIPA buffer supplemented with proteases and phosphatases inhibitors (Sigma). Liver samples were disrupted using TissueLyzer LT (Qiagen) for 3' at 30Hrtz. Lysates were incubated for 30 min on ice and centrifuged for 20 min at maximum speed at 4°C. Supernatant was collected and protein content was determined by Bradford assay (Bio-Rad). Protein samples were separated by SDS-PAGE by using 4%–12% polyacrylamide gels (Bio-Rad). Primary antibody rabbit anti-GFP (Santa Cruz; Cat#sc-8334); mouse anti-β-actin (Novusbio; Cat#NB600-501H) and rabbit p115 (from De Matteis' lab, TIGEM) were diluted in TBS-T (0.8% NaCl, 0.02% KCl, 0.3% Tris-base-0.1% Tween 20)/5% milk (Bio-Rad). Proteins of interest were detected with horseradish peroxidase (HRP)-conjugated goat anti-mouse and goat anti-rabbit IgG antibody (GE Healthcare). Peroxidase substrate was provided by ECL Western Blotting Substrate kit (Pierce).

Shuffled AAV capsid plasmid libraries generation

Development of AAV capsid variants with improved hepatocytes transduction in fibrotic livers was performed as previously reported with minor modifications by directed evolution [51; 52; 64; 65]. Differently from capsid engineering by rational design, directed evolution can be applied without any knowledge of the underlying mechanistic basis. Shuffled *cap* gene libraries were generated starting from 20

parental *cap* genes, including natural and synthetic variants. Based on this approach shuffled *cap* gene libraries have been generated using natural and synthetic AAVs. Briefly, parental *cap* genes underwent fragmentation using DNAseI (Roche) at 1:10 dilution in DNAseI buffer and using 1ug of each *cap* gene per library. Reaction was incubated for 5 minutes at room temperature and loaded on 1,5% agarose gel to evaluate digestion procedure, DNAseI digestion was repeated until fragments reached size between 1000 and 200bp [65]. Fragmentation was interrupted via heat inactivation and fragmented *cap* genes were agarose gel extracted (Qiagen). After DNAseI fragmentation reassembly of the fragments was promoted by a primer-less PCR step, in which they self-prime based on their partial homologies and assembled into chimeric *cap* sequences. Next a primer-less PCR was performed using 500ng of DNAseI-fragmented *cap* genes as a template and Phusion Hot Start Flex DNA Polymerase (NEB) at the following conditions: 30 seconds at 95°C; 40 cycles of 10 seconds at 98°C, 30 seconds at 42°C, 45 seconds at 72°C; 10 minutes at 72°C. Using primers binding to signature region designed outside of *cap* genes we tested various shuffled PCR conditions, the best one was obtained using 0,5uL of unpurified primer-less product with the following conditions: 30 seconds at 98°C; 25 cycles of 10 seconds at 98°C; 15 seconds at 62°C; 1 minutes at 72°C; 10 minutes at 72°C. An additional extension step was performed for 10 minutes at 72°C by diluting shuffled PCR products with two volumes of fresh reaction components. Prior to shuffled *cap* genes gel extraction PCR products were loaded on 1% agarose gel to confirm a band at the molecular weight of 2.200bp. Shuffled PCR products were purified by agarose gel extraction (Qiagen) and used as a template for a second primer PCR that promoted amplification of full-length shuffled variants [66]. PCR products underwent purification using QIaquick PCR purification kit (Quiagen) plus AMPure XP beads (Beckman Culturer) purification and were subcloned into the Zero Blunt™ TOPO™ PCR cloning kit (Invitrogen) to confirm reassembly of the full-length *cap* as well as shuffling of the *cap* genes by Sanger sequencing. Shuffled *cap* genes obtained so far were subcloned in cloned into a replication- and packaging-competent barcoded recipient plasmid, including AAV2 inverted terminal repeats (ITRs), and rep gene [65] using both restriction cloning and ligation-independent cloning method. Random barcodes have also been inserted to easily identify and track AAV variants trough evolution passages [65; 67]. At least twenty of the full-length shuffled *cap* genes obtained underwent single colony isolation and Sanger sequencing to assess reassembly into chimeric capsid.

Shuffled re-assembled *cap* genes cloned into Zero Blunt™ TOPO™ PCR cloning kit (Invitrogen) were restriction digested to perform sticky ends ligation as well as used as template to set up InFusion seamless cloning (Takara Bio) and NEBuilder® HiFi assembly DNA cloning kit (NEB) to achieve subcloning into barcoded recipient plasmid. Stellar™ competent cells (Takara Bio), NEB® 5-alpha competent E. Coli (NEB) and Endura™ electrocompetent cells (Biosearch Technologies) were used for competent cells transformation and subcloning according to the protocol reported by the manufacturer.

Statistical analysis

All statistical analysis were calculated using GraphPad Prism 7. Data comparisons were performed using Student's *t* test, analysis of variance (ANOVA) (one-way or two-way) and area under the curve analysis (AUC) with Sidak's and/or Tukey's multiple comparison test. *P* values of <0.05 were considered significant. Experimental group sizes are reported in the figures as *N* in the caption of each figure. Data are shown as average ± standard error of mean (SEM).

RESULTS

Aim 1: AAV transduction in fibrotic livers

AAV-mediated hepatocyte transduction in acquired model of liver fibrosis

To investigate the effect of liver fibrosis on AAV-mediated gene delivery to hepatocytes TAA was administered to promote liver fibrosis [27]. To this aim, C57BL/6 wild-type mice were treated with increasing doses of TAA for 12 weeks to induce advanced fibrosis/cirrhosis and then intravenously injected with AAV2/8.TBG.eGFP at the dose of $1x10^{13}$ gc/Kg. (Fig. 5). Blood samples were collected at 1-, 6-, 12-, and 24-hours post-injection to evaluate blood clearance rate of AAV vector. Four weeks post-injection organs were harvested for further analysis.

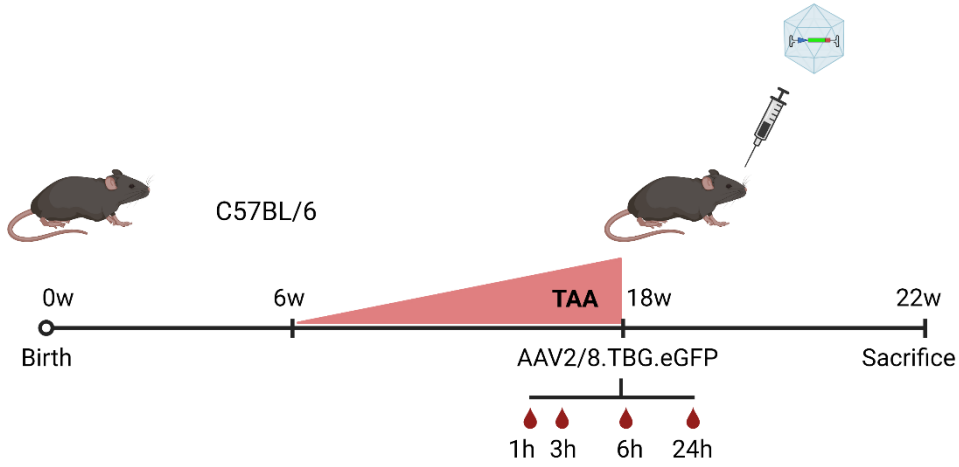

Figure 5: Schematic representation of TAA administration and AAV2/8.TBG.eGFP injection to C57BL/6 mice

Mice were administered with TAA at increasing doses from 6- to 18-weeks of age. At 12 weeks of age TAA was interrupted and AAV2/8.TBG.eGFP was intravenously injected at $1X10^{13}$ gc/Kg. Blood samples were collected at 0-, 1-, 3-, 6- and 24-hours post-injection. Mice were sacrificed 4 weeks post-injection. Image created using BioRender (https://biorender.com/).

We first confirmed liver fibrosis induction by TAA. TAA-treated mice showed increased collagen deposition by Sirius Red staining compared to vehicle treated control mice (Fig. 6A-B).

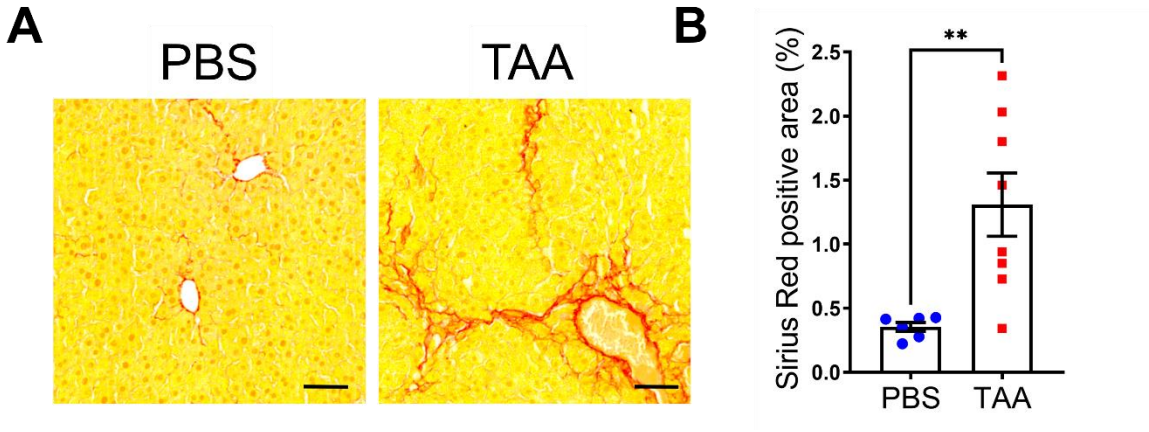

Figure 6: TAA-induced liver fibrosis in C57BL/6 mice

(A) Representative Sirius red staining of N=6 PBS- and N=8 TAA-administered C57BL/6 mice sacrificed at 28 days post-injection. Scale bar: 100µm. (B) Quantification of Sirius red positive area. Data are expressed as percentage over total area. Unpaired t-test. **p<0.01. Data are expressed as mean ±SEM.

Immunofluorescence on liver sections showed reduced GFP expression in TAA- compared to PBS-administered mice (Fig. 7A-B), that was further confirmed by western blot analysis on whole liver lysates (Fig. 7C-D), supporting the hypothesis that liver fibrosis reduces hepatocytes transduction.

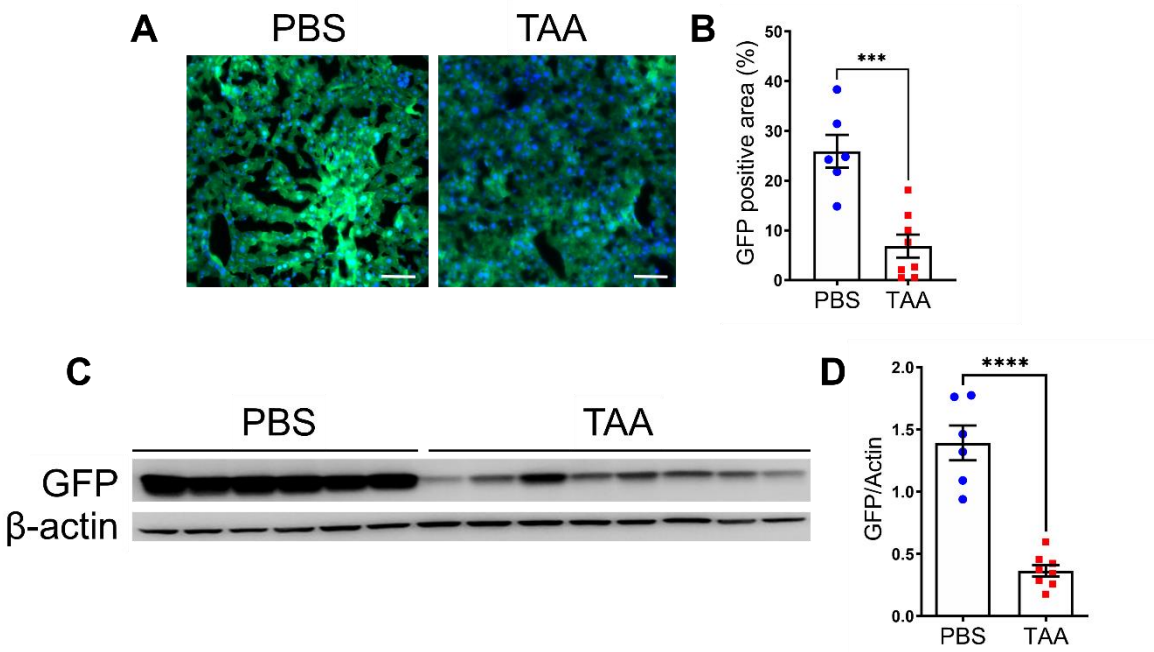

Figure 7: TAA-induced liver fibrosis reduces hepatocyte transduction

(A) Representative immunofluorescence staining on liver sections using anti-GFP antibody of N=6 PBS- and N=8 TAA-administered C57BL/6 mice sacrificed 28 days post-injection. Scale bar: 100µm. (B) Quantification of GFP positive area. Data are expressed as percentage of GFP area normalized to nuclei count. Unpaired t-test analysis. ***p<0.005. (C) Western-blot analysis on liver lysates of

C57BL/6 mice sacrificed 28 days post-injection using anti-GFP antibody. β-actin was used as loading control. (D) Quantification of band intensities in western blot analysis. Unpaired t-test analysis. ****p<0.001. Data are expressed as mean ±SEM.

Impaired hepatocyte transduction was associated with lower hepatic vector genome content in fibrotic mice (Fig. 8).

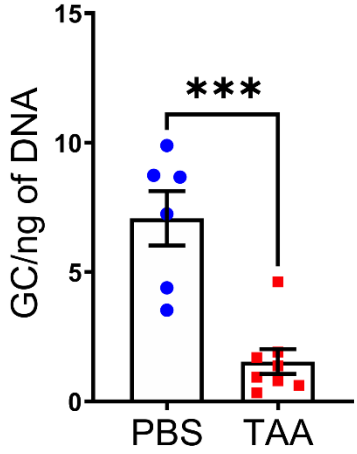

Figure 8: Reduced vector genome content in livers from fibrotic mice

Vector genome copies (GC) in liver by qPCR of N=6 PBS- and N=8 TAA-administered C57BL/6 mice sacrificed 28 days post-injection. Unpaired t-test analysis. ***p<0.005. Data are expressed as mean ±SEM.

Next, vector clearance from the bloodstream was investigated by qPCR analysis of vector genome copies (gc) on serum samples. Serum genome content in non-fibrotic control mice peaked at 1 h post-injection and rapidly declined thereafter. Conversely, TAA-treated mice showed increased blood genome content at 1h post-injection and delayed blood clearance compared to control mice [Area under the curve (AUC): PBS 487,695; TAA 3,080834, t-test: 0.0073] (Fig. 9A), suggesting that liver fibrosis is impairing vector blood clearance. Analysis of extrahepatic organ revealed a trend increase in vector gc in lungs from TAA-treated mice to controls (Fig. 9C), while spleen and bone marrow showed similar vector genome content in fibrotic and non-fibrotic mice (Fig. 9B-D).

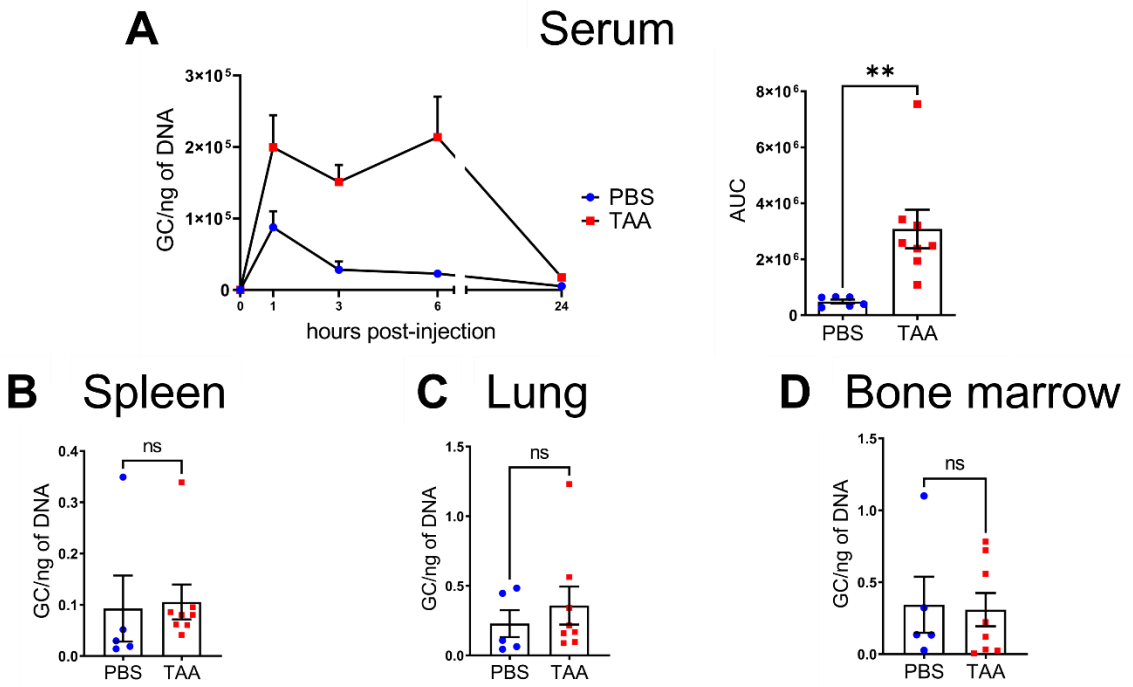

Figure 9: Vector genome content in serum and extra-hepatic organs

(A) Vector genome copies (GC) in serum by qPCR of N=6 PBS- and N=8 TAA-administered C57BL/6 mice. Area under the curve and paired t-test analysis. t-test: **p<0.01. Analysis of vector genome copies by qPCR in (B) spleen, (C) lung and (D) bone marrow of C57BL/6 mice sacrificed 28 days post-injection. Unpaired t-test. Data are expressed as mean ±SEM.

Overall, these data suggested that liver fibrosis strongly impaired hepatocyte transduction by AAV8-based vectors and may result in delayed blood clearance and altered biodistribution.

Liver fibrosis impairs hepatocyte transduction by AAV8 in *Atp7b*$^{-/-}$ mice

We next investigated the impact of fibrosis on AAV-mediated liver-directed gene therapy in a disease-relevant context, using mouse models of inborn errors of metabolism characterized by liver fibrosis. The *Atp7b*$^{-/-}$ mouse [29] recapitulates several features of Wilson disease and has been extensively used to study disease pathogenesis and test novel therapies. In this mouse hepatic copper accumulation starts in the first weeks of life and liver develops steatosis and mild inflammation by six weeks of age, progressing into hepatitis, necroinflammation and extensive perisinusoidal fibrosis by the age of eighteen to twenty weeks [30].

Male 18-week-old *Atp7b*$^{-/-}$ mice and *Atp7b*$^{+/-}$ healthy control mice were intravenously injected with AAV2/8.TBG.eGFP vector at the dose of 5x10^{12} gc/Kg and sacrificed 14 days post-injection to evaluate AAV transduction. At sacrifice, *Atp7b*$^{-/-}$ and *Atp7b*$^{+/-}$ control mice showed increased body weight and a trend increase in liver to

body weight ratio (Fig.10A-B). *Atp7b*$^{-/-}$ livers showed moderate to severe liver fibrosis (Fig 11A-B), that was associated with a significant 50% reduction of GFP^{+} cell number and GFP protein levels compared to controls (Fig.11C-F). Moreover, Pearson's correlation analysis revealed a significant inverse correlation between liver fibrosis and AAV transduction efficiency (Fig. 11G).

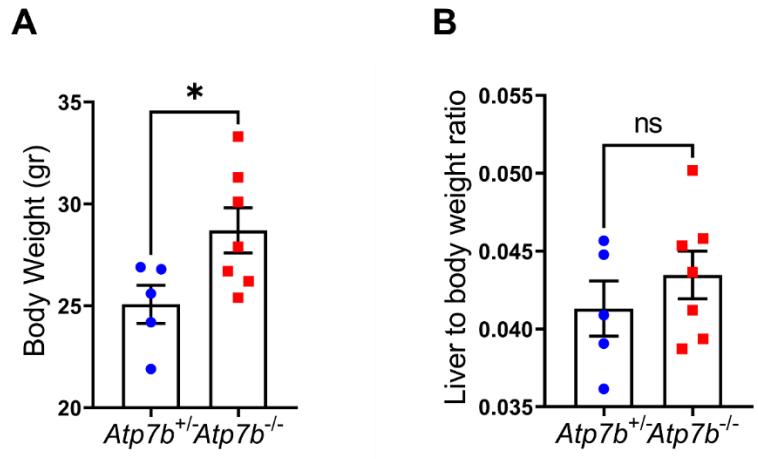

Figure 10: Body weight and liver to body ratio in *Atp7b*$^{-/-}$ mice

Body weight (A)and liver to body weight ratio (B) of N=5 *Atp7b*$^{+/-}$ and N=7 *Atp7b*$^{-/-}$ mice injected with AAV2/8.TBG.eGFP at 18 weeks of age and sacrificed14-days post-injection. t-test analysis. *p<0.05. Data are expressed as mean ±SEM.

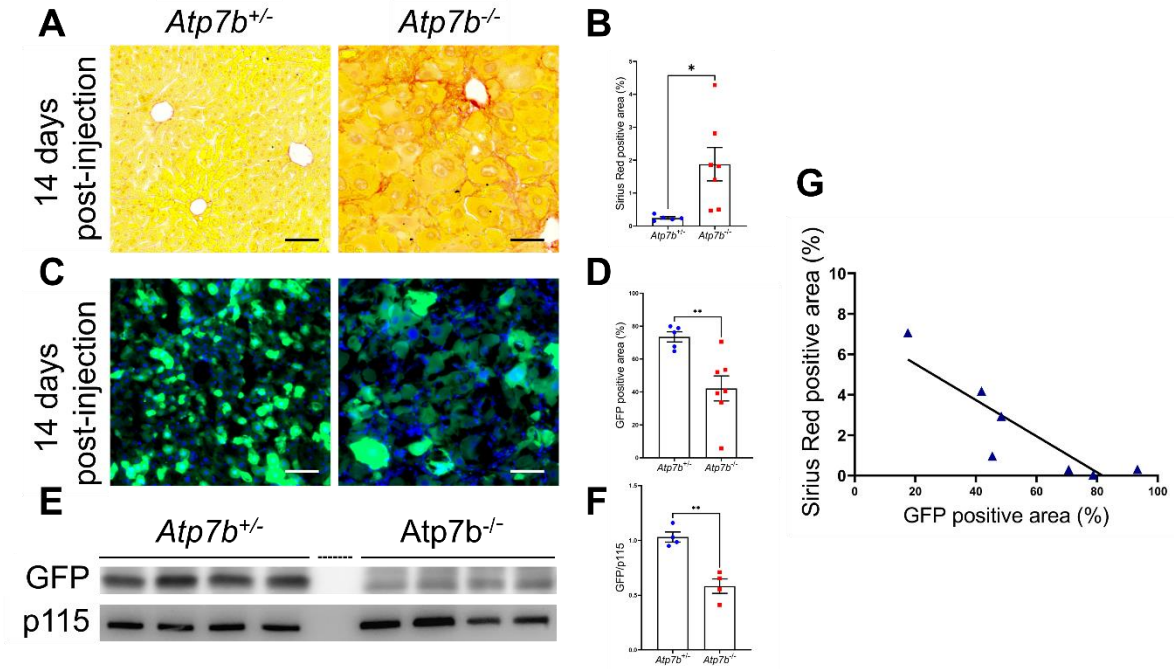

Figure 11: Liver fibrosis impaired hepatocyte transduction in *Atp7b*$^{-/-}$ mice

(A) Representative Sirius red staining of N=5 *Atp7b*$^{+/-}$ and N=7 *Atp7b*$^{-/-}$ mice harvested 14 days post-injection. Scale bar: 100µm. (B) Quantification of Sirius red positive area mice per group. Data are

expressed as percentage over total area. Unpaired t-test analysis. *p<0.05. (C) Representative immunofluorescence staining on liver sections using anti-GFP antibody Scale bar: 100µm. (D). Quantification of GFP positive area. Data are expressed as percentage of GFP area normalized to nuclei count. Unpaired t-test analysis. **p<0.01. (E) Western-blot analysis on liver lysates using anti-GFP antibody. p115 was used as loading control. (F) Quantification of western blot band intensities levels. Unpaired t-test analysis. **p<0.01. (G) Correlation analysis between Sirius red positive area and GFP positive area of N=5 *Atp7b*$^{+/-}$ and N=5 *Atp7*$^{-/-}$ mice per group. Two-tailed correlation analysis. **p<0.01. Data are expressed as mean ±SEM.

Consistent with transduction impairment, vector genome content is reduced in *Atp7b*$^{-/-}$ compared to *Atp7b*$^{+/-}$ livers (Fig. 12).

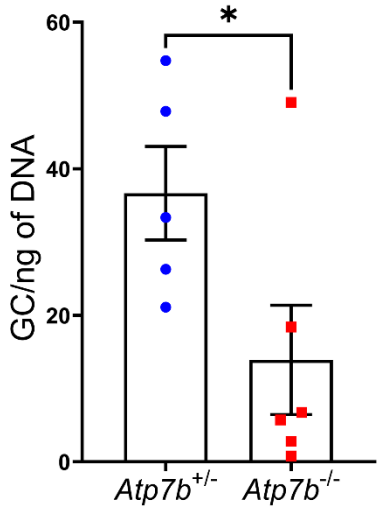

Figure 12: Reduced hepatic vector genome content in fibrotic *Atp7b*$^{-/-}$ mice

Vector genome copies (GC) in liver by qPCR of N=5 Atp7b$^{+/-}$ and N=6 Atp7$^{-/-}$ mice per group. Unpaired t-test analysis. *p<0.05. Data are expressed as mean ±SEM.

Chronic liver damage is usually associated with a regenerative response, and hepatocyte proliferation in response to copper accumulation has been described in *Atp7b*$^{-/-}$ mice [68]. Therefore, we wonder whether reduced transduction efficiency observed at 14 days post-injection was due to reduced vector uptake by the liver or by episomal vector genome dilution over hepatocyte replication cycles. To address this point, we injected *Atp7b*$^{-/-}$ and *Atp7b*$^{+/-}$ mice at 18 weeks of age with the same dose of AAV2/8.TBG.eGFP and sacrificed them after 2 days post-injection to avoid vector dilution effect. Presence of liver fibrosis in *Atp7b*$^{-/-}$ mice was confirmed by Sirius Red staining (Fig. 13).

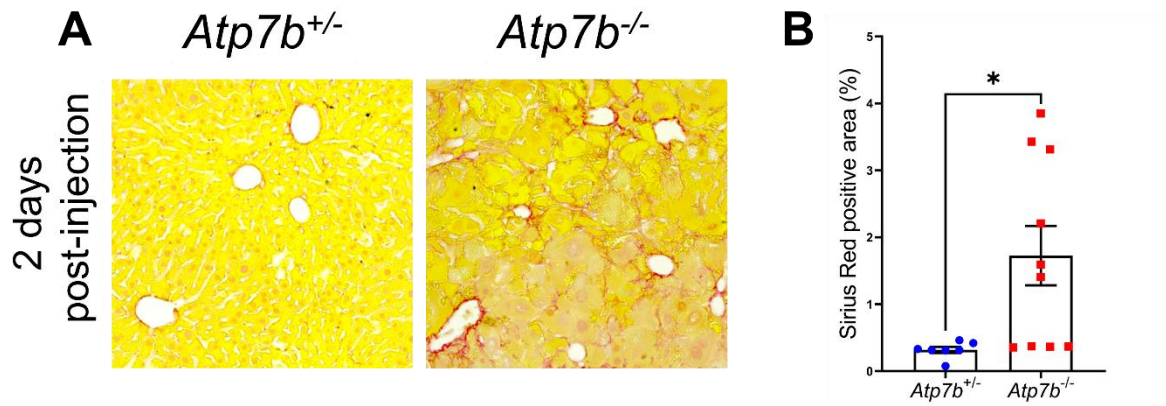

Figure 13: Sirius Red of *Atp7b* mice injected with AAV2/8.TBG.eGFP at 18 weeks of age and harvested 2 days post-injection

Representative Sirius red staining of Atp7b mice harvested 2 days post-injection (A). Quantification of Sirius red positive area of N=7 *Atp7b*$^{+/-}$ and N=10 *Atp7*$^{-/-}$ mice per group. Data are expressed as percentage over total area (B). Data are expressed as mean ±SEM. t-test: *p<0.05.

Analysis of vector blood clearance by qPCR analysis showed a significant increase of circulating vector levels in *Atp7b*$^{-/-}$ mice compared to controls *Atp7b*$^{+/-}$ mice [AUC: *Atp7b*$^{+/-}$: 832,184; *Atp7b*$^{-/-}$: 1,396,217; t-test: 0.0193] (Fig. 14).

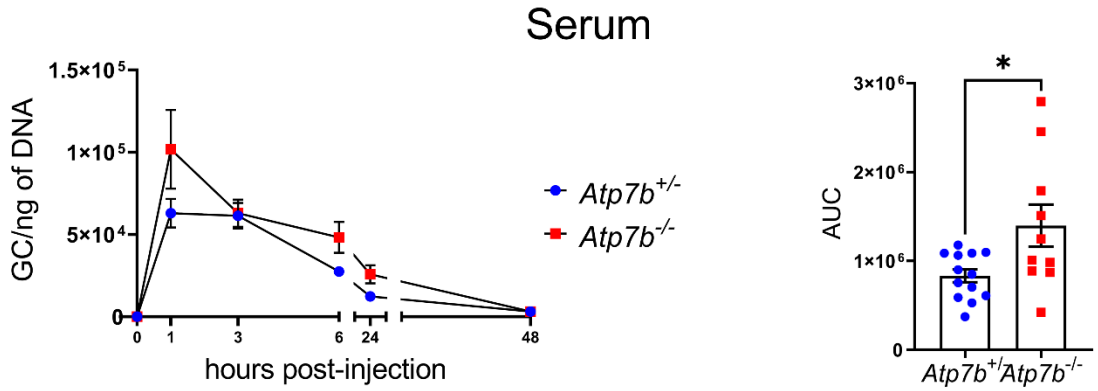

Figure 14: Vector genome copies in serum of *Atp7b* mice injected with AAV2/8.TBG.eGFP

Vector genome copies (GC) in serum by qPCR of N=13 *Atp7b*$^{+/-}$ and N=10 *Atp7*$^{-/-}$ mice. Area under the curve and paired t-test analysis. t-test: *p<0.05. Data are expressed as mean ±SEM.

Nevertheless, mice sacrificed 2 days post-injection revealed a remarkable reduction of hepatic genome content in fibrotic versus non-fibrotic mice (Fig. 15), suggesting that liver fibrosis impaired vector uptake by the liver.

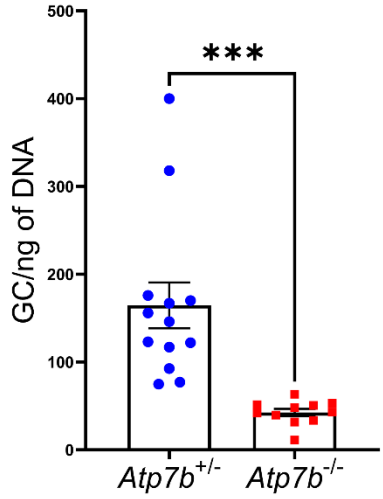

Figure 15: Fibrosis impairs vector uptake by the liver in *Atp7b*$^{-/-}$ mice

Vector genome copies (GC) by qPCR in livers from N=13 *Atp7b*$^{+/-}$ and N=11 *Atp7b*$^{-/-}$ mice. Unpaired t-test analysis. ***p<0.005. Data are expressed as mean ±SEM.

Conversely, *Atp7b*$^{-/-}$ mice showed significantly increased vector genome content in the kidney and a trend increase in lung and brain compared to controls, while a similar vector genome was retrieved from other tested organs in fibrotic and non-fibrotic animals (Fig. 16, A-F).

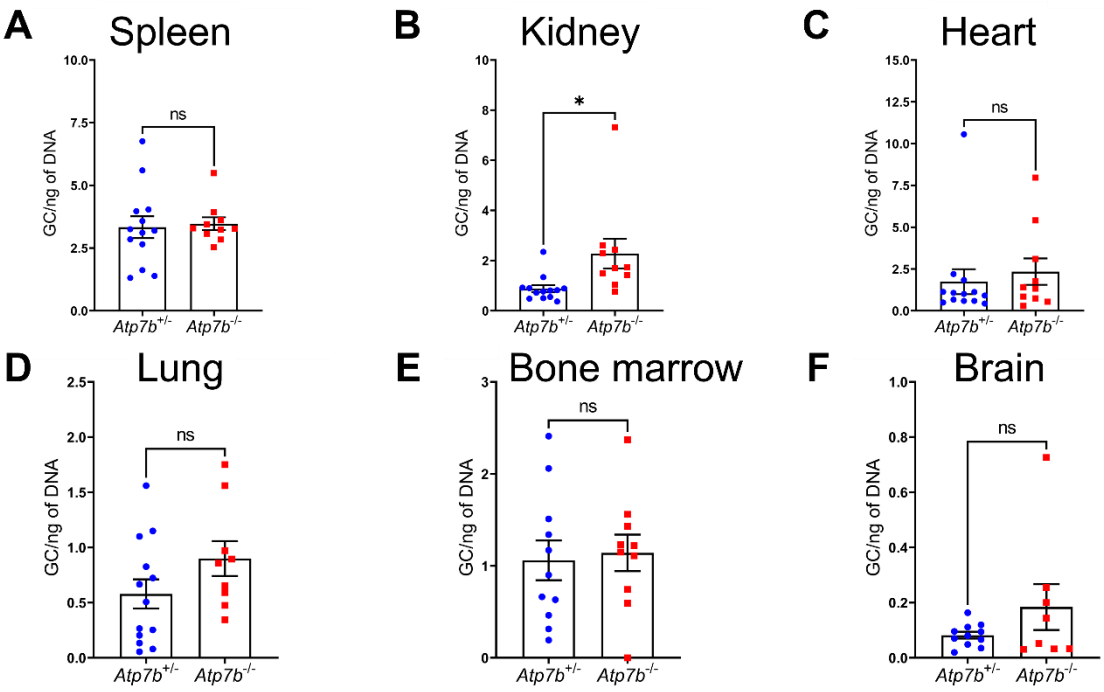

Figure 16: Vector genome content in extra-hepatic organs from *Atp7b*$^{-/-}$ mice

Analysis of vector genome copies (GC) by qPCR in (A) spleen, (B) kidney, (C) heart, (D) lung, (E) bone marrow and (F) brain from N=13 *Atp7b*$^{+/-}$ and N=10 *Atp7b*$^{-/-}$ mice. Unpaired t-test analysis. *p<0.05. Data are expressed as mean ±SEM.

Liver fibrosis impairs hepatocyte transduction by AAV8 and hepatic vector uptake in *Abcb4*$^{-/-}$ mice

To further expand our findings, we investigated AAV8 delivery in *Abcb4*$^{-/-}$ mouse [33] as a widely used model of biliary fibrosis, resembling clinical features of PFIC type 3 and primary sclerosing cholangitis. Since sex significantly influences transduction of murine liver by AAV [69], animals from both sexes were included in this experiment. Male and female *Abcb4*$^{-/-}$ *and Abcb4*$^{+/-}$ control mice were administered with AAV2/8.TBG.eGFP at the dose of 5x10^{12} gc/Kg at 14 or 10 weeks of age, respectively. Animals were sacrificed shortly after injection (2 days) to assess vector biodistribution, and at 14 days post-injection to evaluate transduction efficiency. At sacrifice *Abcb4*$^{-/-}$ mice showed normal body weight (data not shown), while female individuals were characterized by significant hepatomegaly (Fig. 17).

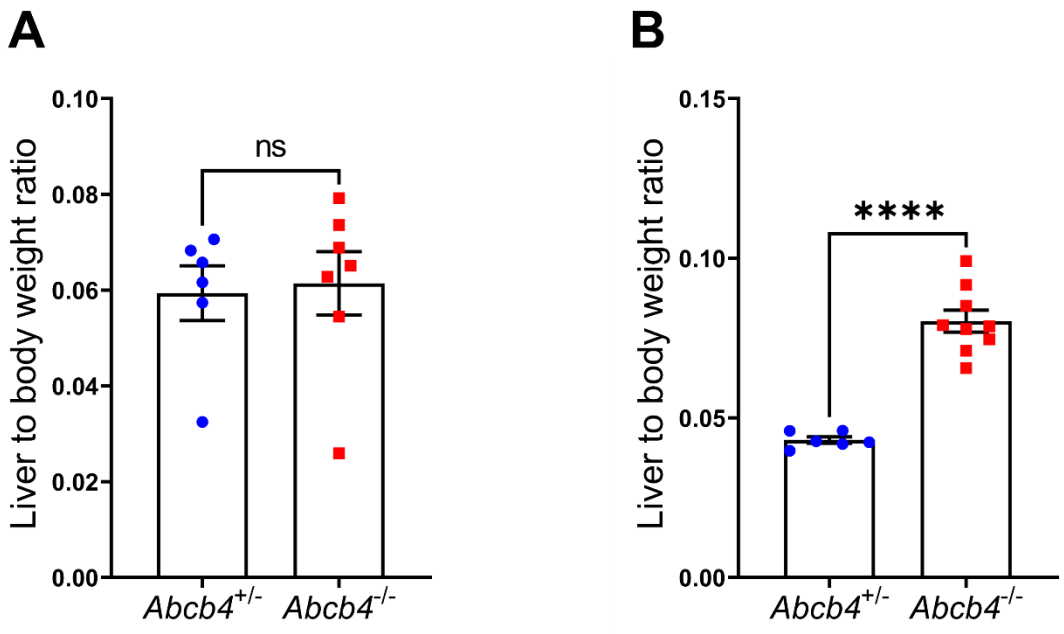

Figure 17: Liver to body ratio in *Abcb4*$^{-/-}$ mice

Liver to body weight ratio of *Abcb4* (A) male and (B) female mice injected with AAV2/8.TBG.eGFP at 10- and 14-weeks of age and sacrificed 14-days post-injection respectively. Mice groups were composed of N=6 *Abcb4*$^{+/-}$ and N=7 *Abcb4*$^{-/-}$ male mice and of N=6 *Abcb4*$^{+/-}$ and N=9 *Abcb4*$^{-/-}$ mice sacrificed 14 days post-injection. Unpaired t-test analysis. ****p<0.001. Data are expressed as mean ±SEM.

Sirius red analysis confirmed significant biliary fibrosis in *Abcb4*$^{-/-}$ mice (Fig. 18A-D and Fig. 19A-D), that was associated with a significant reduction of transduction efficiency at 14 days post-injection in both male and female mice (Fig. 18E-F and Fig. 19E-F).

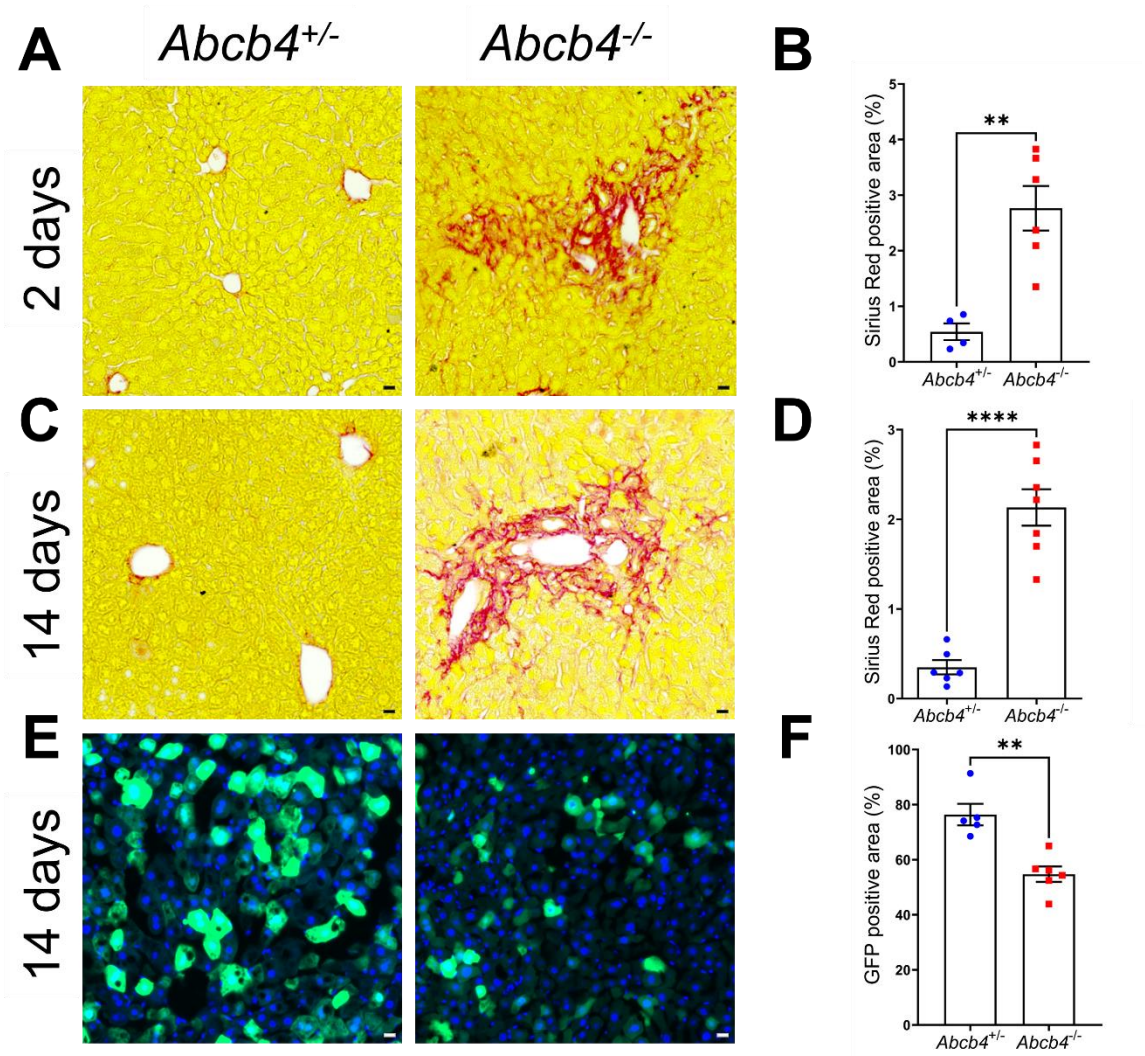

Figure 18: Liver fibrosis impaired hepatocyte transduction in male *Abcb4*$^{-/-}$ mice

(A) Representative Sirius red staining of N=4 *Abcb4*$^{+/-}$ and N=6 *Abcb4*$^{-/-}$ male mice harvested 2 days post-injection. Scale bar: 100µm. (B) Quantification of Sirius red positive area per group. Data are expressed as percentage over total area. Unpaired t-test analysis. **p<0.01. (C) Representative Sirius red staining of of N=6 *Abcb4*$^{+/-}$ and N=7 *Abcb4*$^{-/-}$ male mice harvested 14 days post-injection. Scale bar: 100µm. (D) Quantification of Sirius red positive area per group. Data are expressed as percentage over total area. Unpaired t-test analysis. ****p<0.001. (E) Representative immunofluorescence staining on liver sections from N=5 *Abcb4*$^{+/-}$ and N=6 *Abcb4*$^{-/-}$ male mice harvested 14 days post-injection using anti-GFP antibody. Scale bar: 100µm. (F) Quantification of GFP positive area. Data are expressed as percentage of GFP area normalized to nuclei count. Unpaired t-test analysis. **p<0.01. Data are expressed as mean ±SEM.

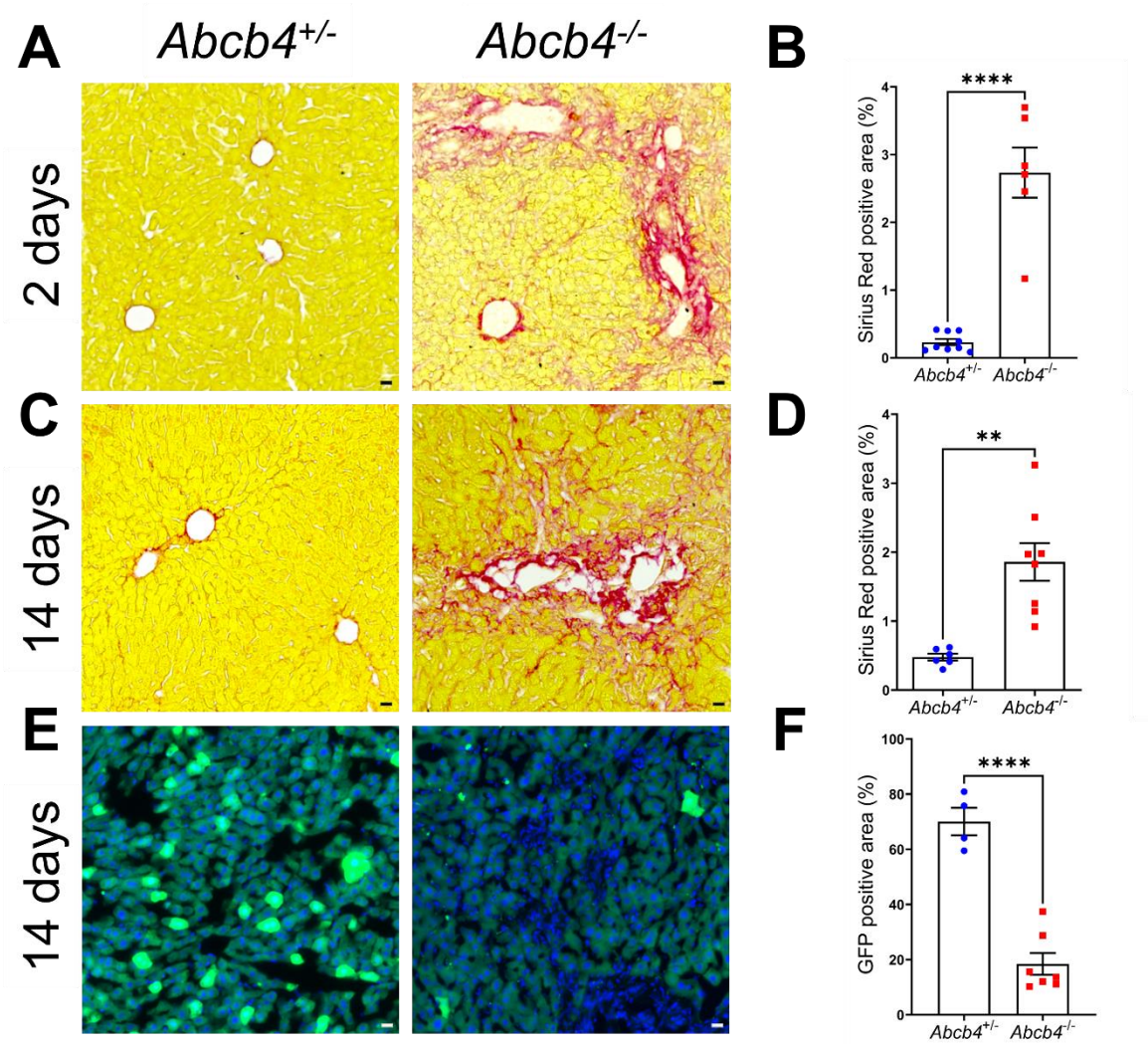

Figure 19: Liver fibrosis impaired hepatocyte transduction in female *Abcb4*$^{-/-}$ mice

(A) Representative Sirius red staining of N=9 *Abcb4*$^{+/-}$ and N=6 *Abcb4*$^{-/-}$ female mice harvested 2 days post-injection. Scale bar: 100µm. (B) Quantification of Sirius red positive area. Data are expressed as percentage over total area. Unpaired t-test-analysis. **p<0.01. (C) Representative Sirius red staining of N=6 *Abcb4*$^{+/-}$ and N=8 *Abcb4*$^{-/-}$ female mice harvested 14 days post-injection. Scale bar: 100µm. (D) Quantification of Sirius red positive area. Data are expressed as percentage over total area. Unpaired t-test-analysis. ****p<0.001. (E) Representative immunofluorescence staining on liver sections of N=4 *Abcb4*$^{+/-}$ and N=7 *Abcb4*$^{-/-}$ female mice harvested 14 days post-injection using anti-GFP antibody. Scale bar: 100µm. (F) Quantification of GFP-positive area. Data are expressed as percentage of GFP area normalized to nuclei count. Unpaired t-test-analysis. **p<0.01. Data are expressed as mean ±SEM.

Analysis of hepatic vector genome content revealed a 60% reduction in *Abcb4*$^{-/-}$ male mice over controls, that was sustained up to 14 days post-injection (Fig. 20A). Female *Abcb4*$^{-/-}$ mice showed a trend reduction of hepatic genome content versus control mice at 2 days post-injection, that was further increased at 14 days post-injection (Fig. 20B).

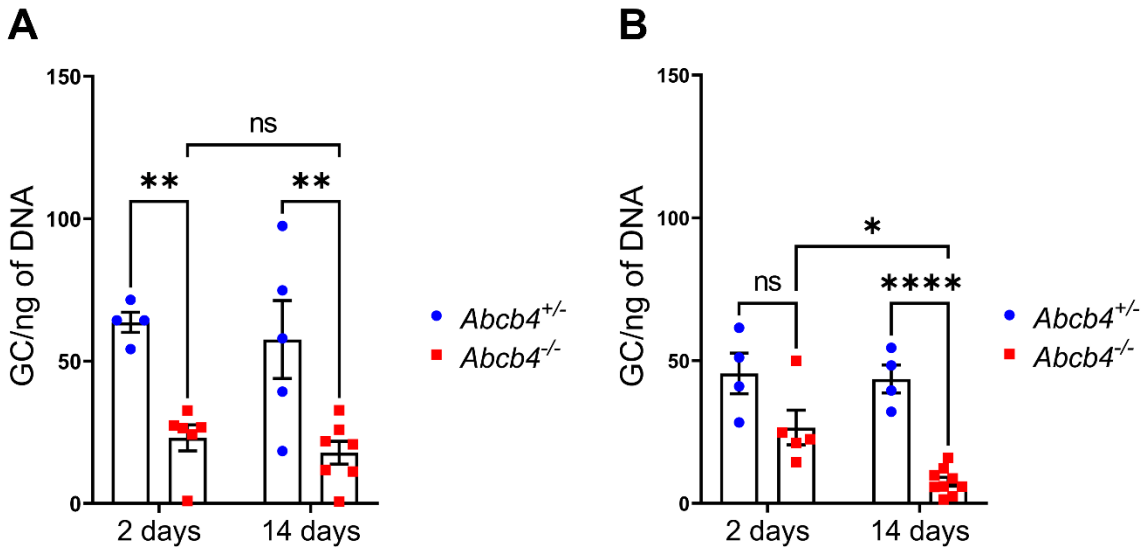

Figure 20: Liver fibrosis reduces liver vector uptake in *Abcb4*$^{-/-}$ mice

(A) Vector genome copies (GC) by qPCR in livers from N=4 *Abcb4*$^{+/-}$ and N=6 *Abcb4*$^{-/-}$ male mice harvested 2 days post-injection and N=5 *Abcb4*$^{+/-}$ and N=7 *Abcb4*$^{-/-}$ male mice harvested 14 days post-injection. (B) Vector genome copies (GC) by qPCR in livers from N=4 *Abcb4*$^{+/-}$ and N=5 *Abcb4*$^{-/-}$ female mice harvested 2 days post-injection and of N=4 *Abcb4*$^{+/-}$ and N=9 *Abcb4*$^{-/-}$ female mice harvested 14 days post-injection mice. Two-way ANOVA plus Tukey's post-hoc analysis: *p<0.05; **p<0.01; ****p<0.001. Data are expressed as mean ±SEM.

Analysis of vector blood clearance showed similar kinetics in *Abcb4*$^{-/-}$ and control male mice, although *Abcb4*$^{-/-}$ mice showed a non-significant decrease of blood peak concentration at 1h post-injection [AUC: *Abcb4*$^{+/-}$: 1,263358*; Abcb4*$^{-/-}$: 1,483789; t-test: 0.5772] (Fig. 21A). Surprisingly, *Abcb4*$^{-/-}$ female mice showed greatly increased vector clearance rate compared to controls [AUC: *Abcb4*$^{+/-}$: 2,758585*; Abcb4*$^{-/-}$: 741,446; t-test: 0.0184] (Fig. 21B), thus suggesting increased vector clearance from the bloodstream.

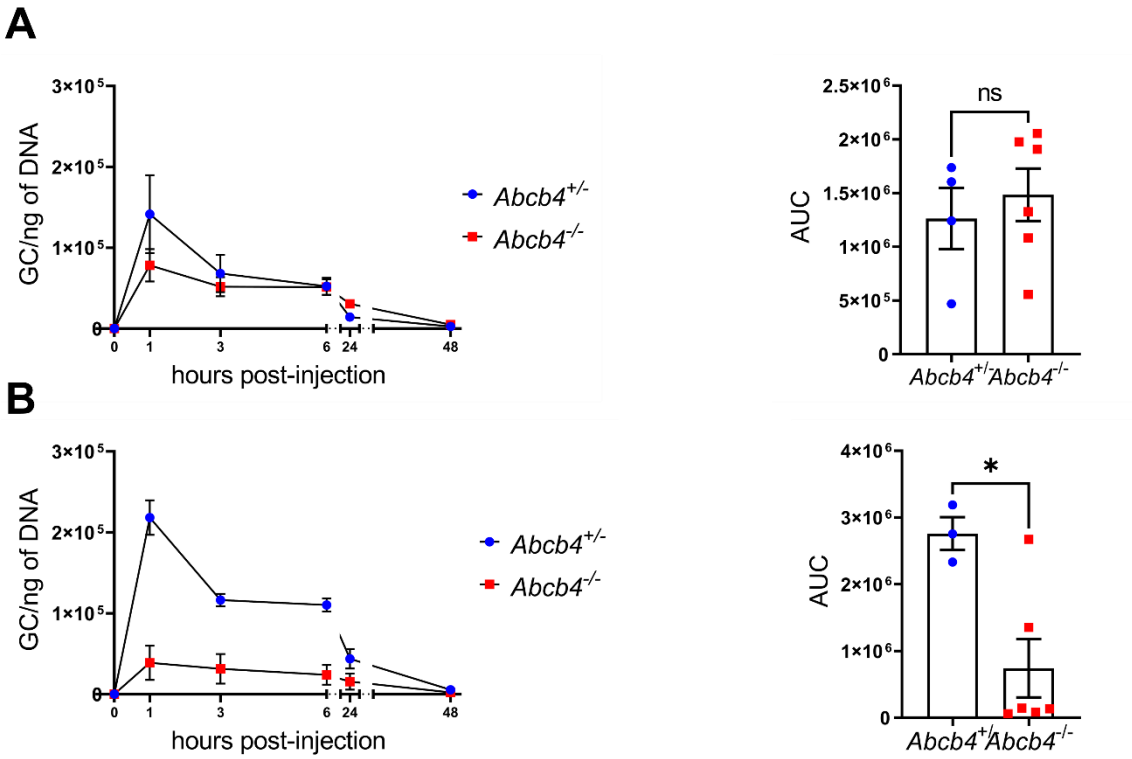

Figure 21: Vector genome copies in plasma of *Abcb4* male and female mice injected with AAV2/8.TBG.eGFP

(A) Vector genome copies (GC) in plasma by qPCR of N=4 *Abcb4*$^{+/-}$ and N=6 *Abcb4*$^{-/-}$ male mice per group. Area under the curve and paired t-test analysis. (B) Vector genome copies (GC) in plasma by qPCR of N=8 *Abcb4*$^{+/-}$ and N=6 *Abcb4*$^{-/-}$ female mice per group. Area under the curve and paired t-test analysis. t-test: *p<0.05. Data are expressed as mean ±SEM.

Next, vector genome content was evaluated in extra-hepatic organs to assess overall AAV8 biodistribution. Fibrotic *Abcb4*$^{-/-}$ male mice showed a significant increase of vector genome content in spleen, a trend increase in heart, lung, bone marrow and brain and no significative differences in kidney, (Fig. 22).

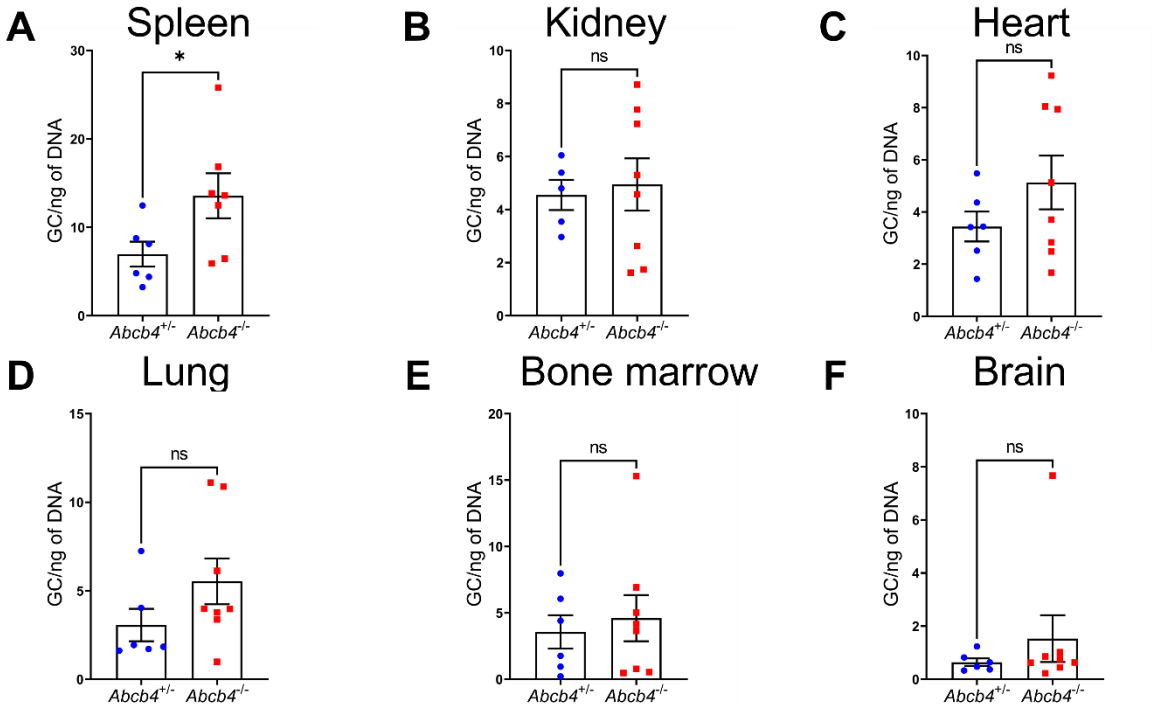

Figure 22: Vector biodistribution in extra-hepatic organs in *Abcb4*$^{-/-}$ male mice

Analysis of vector genome copies (GC) by qPCR in (A) spleen, (B) kidney, (C) heart, (D) lung, (E) bone marrow and (F) brain in N=6 *Abcb4*$^{+/-}$ and N=8 *Abcb4*$^{-/-}$ male mice. Unpaired t-test analysis. Data are expressed as mean ±SEM.

Female fibrotic mice showed a non-significant increase versus non-fibrotic mice in genome content in spleen and kidney, while we found a trend reduction in other tested organs (Fig. 23).

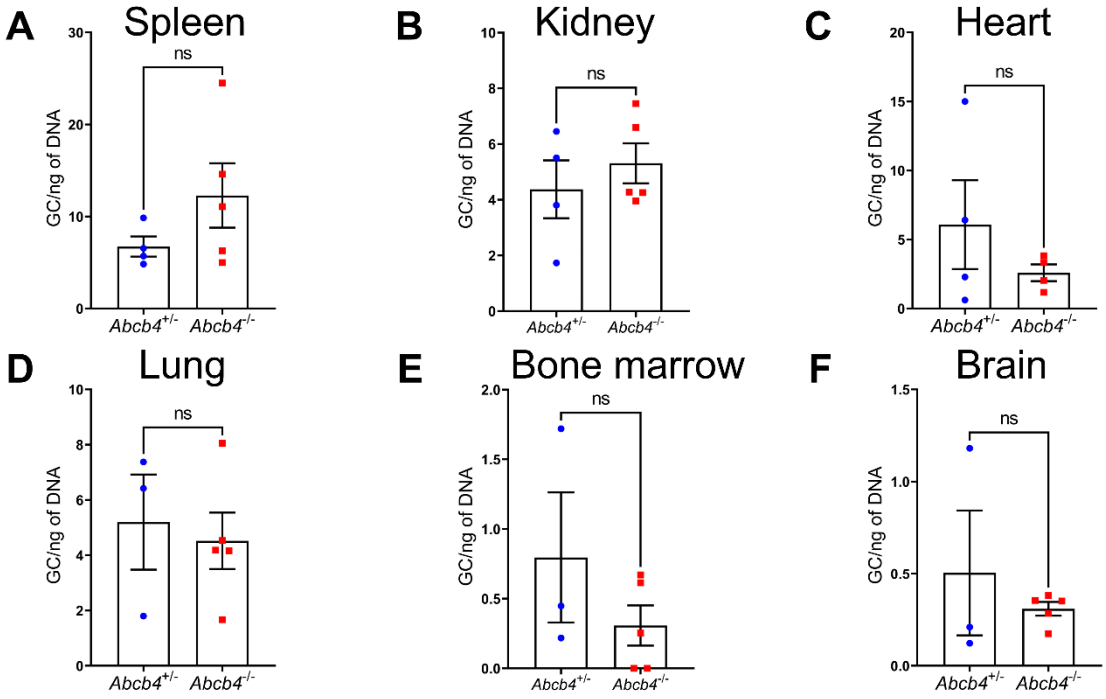

Figure 23: Vector biodistribution in extra-hepatic organs in *Abcb4*$^{-/-}$ female mice

Analysis of vector genome copies (GC) by qPCR in (A) spleen, (B) kidney, (C) heart, (D) lung, (E) bone marrow, and (F) brain in N=3 *Abcb4*$^{+/-}$ and N=5 *Abcb4*$^{-/-}$ female mice. Unpaired t-test analysis. Data are expressed as mean ±SEM.

Aim 2: Development of novel synthetic AAVs with improved hepatocyte transduction in fibrotic livers

Current knowledge about the interaction of the AAV capsid with the fibrotic tissue is insufficient to enable the rational design of new variants. Differently from capsid engineering by rational design, directed evolution can be applied without any knowledge of the underlying mechanistic basis.

Experimental strategy

Parental *cap* will undergo DNAseI fragmentation and reassembly by a primer-less PCR step, in which they self-prime based on their partial homologies and assembled into chimeric *cap* sequences. A second primer PCR will promote amplification of full-length shuffled variants [66] that will be cloned into a replication- and packaging-competent barcoded recipient plasmid, including AAV2 inverted terminal repeats (ITRs), and rep gene [65]. Random barcodes have also been inserted to easily identify and track AAV variants trough evolution passages [65; 67]. Before vector particle production, at least twenty of the full-length shuffled *cap* genes obtained will undergo

single colony isolation and Sanger sequencing to assess reassembly into chimeric capsid. Next, library integrity and diversity will be further analyzed by NGS using PacBio technology [70]. AAV library will be produced and intravenously injected into fibrotic *Atp7b*$^{-/-}$ and *Abcb4*$^{-/-}$ mice. After a week, livers will be harvested, hepatocytes will be isolated and genomic DNA will be extracted. Genomic DNA will be PCR amplified, repackaged into AAVs and re-administered to mice. Rounds of selection will be repeated at least 3 times or until enrichment of AAV variants will emerge [52]. Sequence of *cap* genes from yielded variants will be analyzed by NGS. Evolved variants will be individually tested for hepatocyte transduction in fibrotic *Abcb4*$^{-/-}$ and *Atp7b*$^{-/-}$ mice and benchmarked against AAV8. Finally, AAV variants will be screened against pooled normal human sera, to test their ability to evade neutralization. Experimental strategy for this aim is summarized in Fig. 24.

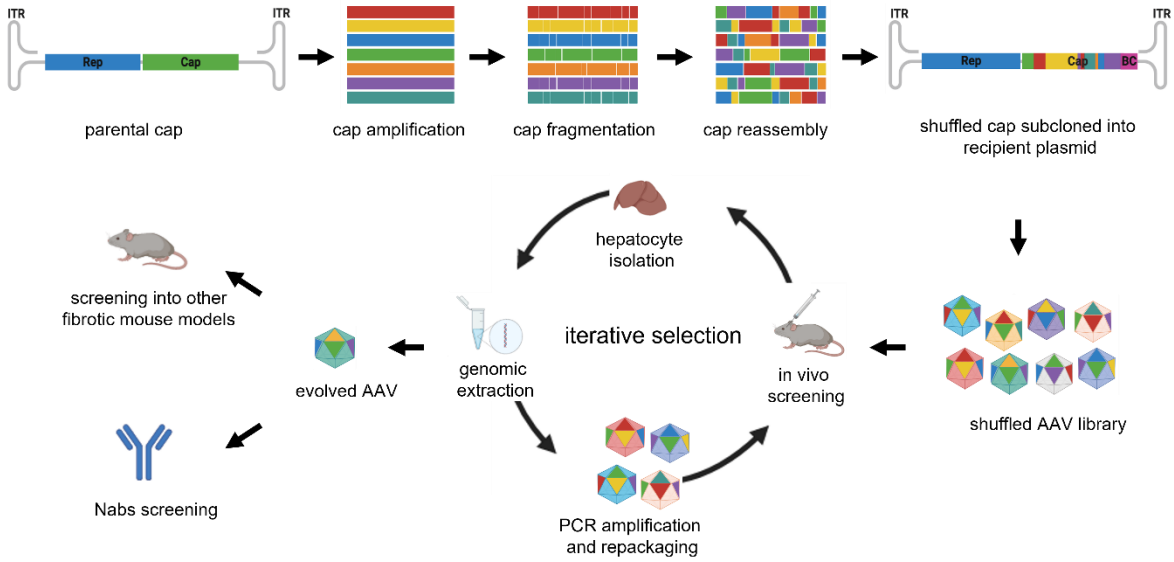

Figure 24: Illustrative workflow of directed evolution strategies used to develop novel AAV variants.

Image created using BioRender (https://biorender.com/)

Shuffled *cap* libraries generation

To generate shuffled *cap* libraries, we gathered 20 parental *cap* genes belonging from natural and synthetic variants. We aimed at generating three different libraries: a complete one (referred to as FULL library throughout the thesis), including the entire repertoire of available 20 *cap* variants (Fig. 25); a second one, encompassing natural and synthetic variants, including *cap* exhibiting the highest degree of nucleotide homology (referred to as HOMO library from now on and shown in red in Fig. 25); a third one including *cap* genes from AAV variants isolated in pigs the most

divergent natural serotype AAV5 (referred to as PIG library and depicted in green in Fig. 25).

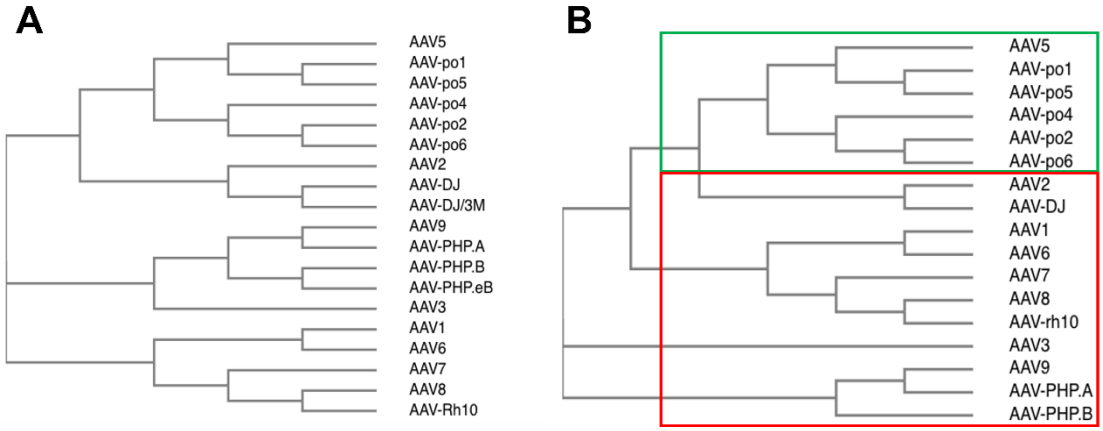

Figure 25: Genealogical relationship at the DNA level of AAV variants used to generate shuffled *cap* libraries.

FULL shuffled *cap* library, including complete repertoire of *cap* genes available (A). PIG library encompassing porcine variants and AAV5 (B, shown in green). HOMO library, including natural and engineered serotypes (B, shown in red). Image created using Clustal Omega (https://www.ebi.ac.uk/Tools/msa/clustalo/).

To generate the shuffled *cap* library a recipient pAAV plasmid has been engineered to contain the AAV2 ITRs and *rep* gene, encoding AAV replication proteins, and a synthetic multi-cloning site downstream to the *rep* gene, to accommodate shuffled *cap* genes. Additionally, unique barcodes (BCs) have been cloned downstream to the *cap* polyadenylation signal. Diversity of barcoded plasmid library has been confirmed by Sanger sequencing of several individual clones (data not shown). We performed DNAseI fragmentation of parental *cap* genes to generate FULL (Fig. 26A), HOMO and PIG shuffled *cap* library (data not shown) and successfully executed primer-less and primer PCR to promote shuffled full-length re-assembly (Fig. 26B).

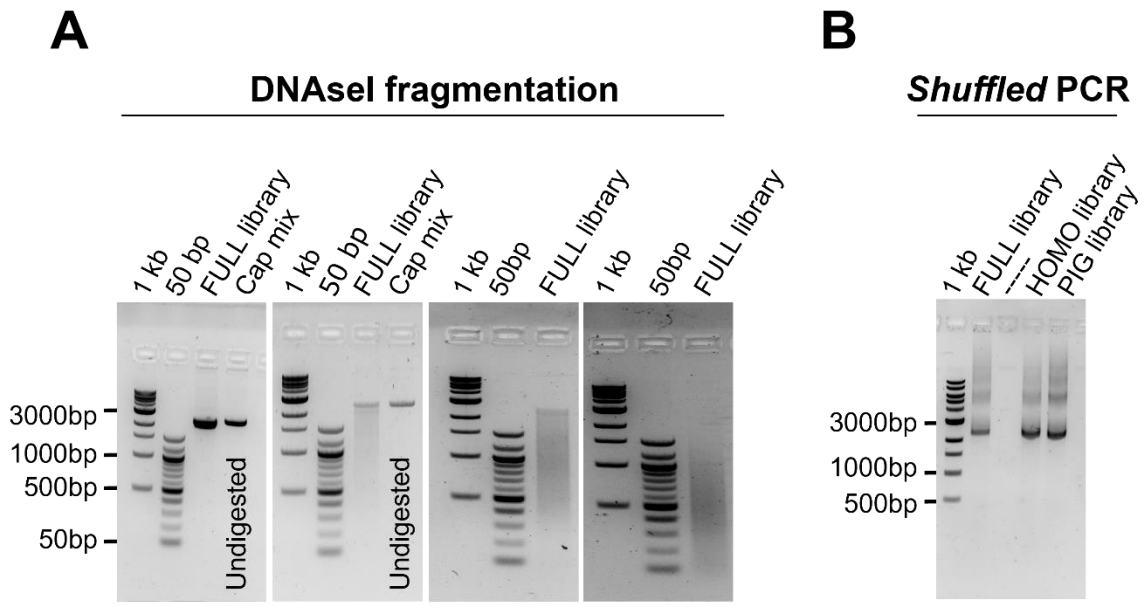

Figure 26: DNAseI fragmentation and reassembly of shuffled *cap* libraries

DNAseI fragmentation of FULL library and mixed undigested parental *cap* loaded on agarose gel for fragmentation process monitoring overtime (A, left panel). Fragmentation was interrupted when mixed *cap* reached size between 1000bp and 200 bp (A, right panel). Shuffled PCR of DNAseI fragmented *cap* as a template of FULL, HOMO and PIG library band at the expected molecular weight of 2200bp (B).

Shuffled re-assembled *cap* were purified and subcloned in barcoded recipient plasmid using different chemically and electrocompetent strains. Yield of the shuffled libraries obtained was approximately 200 species in FULL, 400 species in HOMO and 100 species in PIG.

To increase shuffled libraries yield we subcloned shuffled libraries into TOPO cloning kit we sequenced sequence portion of the shuffled *cap* and confirmed *cap* re-assembling and integrity of common *cap* extremities, which are needed for cloning. Next, we sequenced the barcoded recipient plasmid and verified the conservation of restriction sites. Sanger sequence confirmed appropriate sequence of the restriction sites essential for cloning. Cloning of shuffled *cap* in the recipient pAAV plasmid is currently ongoing.

DISCUSSION

AAV-based vectors are the most promising tools for liver directed gene therapy due to their ability to transduce diving and non-dividing cells, high safety profile, low immunogenicity and long-term expression of the transgene. However, knowledge on AAV vector interactions with fibrotic livers are still very limited. Here we investigated AAV mediated gene therapy infection and transduction in induced and genetic-based liver fibrosis animal models.

Using three mouse models characterized by different types of liver fibrosis, we provided compelling evidence that livers are transduced less efficiently by AAV8-based vectors in presence of fibrosis. This was a common finding across the tested models, irrespective of fibrosis pattern and etiology, and is consistent with previous studies in *Abcb4*$^{-/-}$ and *Atp7b*$^{-/-}$ mice, showing a remarkable reduction in AAV8-mediated transgene expression and therapeutic efficacy when injected after liver fibrosis development [61; 62].

Notably, previous studies also highlighted the importance of hepatocyte proliferation in response to damage resulting in transgene loss and decline of therapeutic efficacy [71]; [72]. Hepatocyte proliferation can impact on vector genome concentration very rapidly, as illustrated by the significant decrease of vector genome copies in the livers of female *Abcb4*$^{-/-}$ mice at 14 days compared to 2 days after vector administration. Nevertheless, decreased vector genome content in fibrotic compared non-fibrotic livers was already observed at 2 days post-injection, a very short time-window in which dilution effect is supposed to be negligible, strongly suggesting that liver fibrosis impaired vector uptake by livers cells.

Physical barriers posed by fibrosis to hepatocyte transduction such as deposition of ECM in the perisinusoidal space [71], or loss of SEC fenestration [53] may reduce vector uptake by the liver and delay blood vector clearance, as shown by *Atp7b*$^{-/-}$ and TAA-treated mice. Biodistribution analysis suggested that persistent AAV circulation in the bloodstream results in a non-specific distribution of viral particle in extrahepatic organs. Conversely, despite reduced hepatic vector genome content, vector clearance rate was increased in *Abcb4*$^{-/-}$ mice. This was paralleled by a significant increase of vector uptake by the spleen, associated to a milder, non-significant increase of vector genome content in other extra-hepatic organs. Like the liver, spleen is involved in immune homeostasis and pathogen clearance from

bloodstream [73]. Red pulp provide filtering function while white pulp, mainly composed of nodules of lymphoid tissues, is involved in immunological defense against bloodborne antigens [74]. Liver and spleen are connected by portal circulation and have relevant crosstalk. Liver fibrosis induces portal hypertension which may lead to congestion of portal system causing splenomegaly [73], and enhance the number and the phagocytic activity of splenic macrophages in the red pulp and marginal zone, resulting in hypersplenism [73]. Blood-engorgement and increased scavenging of viral particles by resident macrophages may contribute to increased vector uptake by the spleen. Splenomegaly has been reported in *Abcb4*$^{-/-}$ mice [33], but is also a recognized feature of *Atp7b*$^{-/-}$ mice [75] that did not show increased vector genomes in the spleen compared to controls. This suggested that some disease-specific alteration of spleen structure and/or function resulting from ABCB4-deficiency may be responsible for enhanced vector uptake. Noteworthy, hepato- and splenomegaly may also have an impact on quantification of vector genome content.

Our study investigated bulk hepatic vector content, although altered fibrotic liver cellularity, characterized by activation and proliferation of HSC, KC and other white cells and significant modifications of SECs, must be also considered [54; 55; 56.]. Vector uptake by NPCs may be increased in fibrotic conditions, resulting in vector degradation and weak or no transgene expression by hepatocyte-specific promoters. Further studies are clearly needed to investigate cell-type specific uptake of blood-borne AAV particles in the context of liver fibrosis. Importantly, increased vector uptake by immune-competent cells in liver and spleen may also enhance vector immunogenicity [54, 55], significantly reducing AAV safety.

According to our study, a higher vector dose should be needed to achieve a therapeutic benefit in patients with liver fibrosis. However, high vector doses have been associated with sever adverse events [76] and death in presence of pre-existing liver damage [77]. Clearly, better vectors are needed to achieve the goal of effective and safe gene therapy for diseases with liver fibrosis.

We proposed to generate novel capsid variants with improved hepatocyte transduction in fibrotic livers by directed evolution of shuffled capsid libraries. Reconstitution efficiency of a shuffled library is a function of sequence homology of parental genes and reassembly is more efficient in presence of more than 80% of sequence homology [51], [67]. Because of these limitations, we generated three different libraries to minimize low *cap* reconstitution efficiency. Nevertheless, the number of species generated is still quite low. We are currently working at improving the yield

of shuffled *cap* reconstitution and at efficiently cloning the *cap* library in the production plasmid.

CONCLUSIONS

Outcome of gene therapy in patients with overt liver fibrosis is currently hard to predict. This work highlighted this neglected aspect of liver-directed gene therapy and provide information that may have an impact on ongoing and future clinical trials. While clearly indicating that liver fibrosis significantly alters AAV8 biodistribution and hepatic transduction efficiency, our work paved the way for future studies aimed at investigating fibrosis impact on vector safety and effect on other AAV variants.

REFERENCES

1. Papanikolaou E, Bosio A. The Promise and the Hope of Gene Therapy. *Front Genome Ed*. 2021;3:618346. doi:10.3389/fgeed.2021.618346

2. Chira S, Jackson CS, Oprea I, et al. Progresses towards safe and efficient gene therapy vectors. *Oncotarget*. 2015;6(31):30675-30703. doi:10.18632/oncotarget.5169

3. Lundstrom K. Viral Vectors in Gene Therapy. *Diseases*. 2018;6(2):42. doi:10.3390/diseases6020042

4. Li C, Samulski RJ. Engineering adeno-associated virus vectors for gene therapy. *Nat Rev Genet*. 2020;21(4):255-272. doi:10.1038/s41576-019-0205-4

5. Sonntag F, Köther K, Schmidt K, et al. The Assembly-Activating Protein Promotes Capsid Assembly of Different Adeno-Associated Virus Serotypes. *J Virol*. 2011;85(23):12686-12697. doi:10.1128/JVI.05359-11

6. Galibert L, Hyvönen A, Eriksson RAE, et al. Functional roles of the membrane-associated AAV protein MAAP. *Sci Rep*. 2021;11(1):21698. doi:10.1038/s41598-021-01220-7

7. Xie Q, Bu W, Bhatia S, et al. The atomic structure of adeno-associated virus (AAV-2), a vector for human gene therapy. *Proc Natl Acad Sci*. 2002;99(16):10405-10410. doi:10.1073/pnas.162250899

8. Agbandje-McKenna M, Kleinschmidt J. AAV Capsid Structure and Cell Interactions. In: Snyder RO, Moullier P, eds. *Adeno-Associated Virus*. Vol 807. Methods in Molecular Biology. Humana Press; 2012:47-92. doi:10.1007/978-1-61779-370-7_3

9. Kotterman MA, Schaffer DV. Engineering adeno-associated viruses for clinical gene therapy. *Nat Rev Genet*. 2014;15(7):445-451. doi:10.1038/nrg3742

10. Wang D, Tai PWL, Gao G. Adeno-associated virus vector as a platform for gene therapy delivery. *Nat Rev Drug Discov*. 2019;18(5):358-378. doi:10.1038/s41573-019-0012-9

11. Flotte TR. Gene Therapy Progress and Prospects: Recombinant adeno-associated virus (rAAV) vectors. *Gene Ther*. 2004;11(10):805-810. doi:10.1038/sj.gt.3302233

12. Pillay S, Carette JE. Host determinants of adeno-associated viral vector entry. *Curr Opin Virol*. 2017;24:124-131. doi:10.1016/j.coviro.2017.06.003

13. Bartlett JS, Wilcher R, Samulski RJ. Infectious Entry Pathway of Adeno-Associated Virus and Adeno-Associated Virus Vectors. *J Virol*. 2000;74(6):2777-2785. doi:10.1128/JVI.74.6.2777-2785.2000

14. Xiao PJ, Samulski RJ. Cytoplasmic Trafficking, Endosomal Escape, and Perinuclear Accumulation of Adeno-Associated Virus Type 2 Particles Are

Facilitated by Microtubule Network. *J Virol*. 2012;86(19):10462-10473. doi:10.1128/JVI.00935-12

15. Sonntag F, Bleker S, Leuchs B, Fischer R, Kleinschmidt JA. Adeno-Associated Virus Type 2 Capsids with Externalized VP1/VP2 Trafficking Domains Are Generated prior to Passage through the Cytoplasm and Are Maintained until Uncoating Occurs in the Nucleus. *J Virol*. 2006;80(22):11040-11054. doi:10.1128/JVI.01056-06

16. Xiao W, Warrington KH, Hearing P, Hughes J, Muzyczka N. Adenovirus-Facilitated Nuclear Translocation of Adeno-Associated Virus Type 2. *J Virol*. 2002;76(22):11505-11517. doi:10.1128/JVI.76.22.11505-11517.2002

17. Fisher KJ, Gao GP, Weitzman MD, DeMatteo R, Burda JF, Wilson JM. Transduction with recombinant adeno-associated virus for gene therapy is limited by leading-strand synthesis. *J Virol*. 1996;70(1):520-532. doi:10.1128/jvi.70.1.520-532.1996

18. Duan D, Yan Z, Yue Y, Engelhardt JF. Structural Analysis of Adeno-Associated Virus Transduction Circular Intermediates. *Virology*. 1999;261(1):8-14. doi:10.1006/viro.1999.9821

19. Chandler RJ, LaFave MC, Varshney GK, Burgess SM, Venditti CP. Genotoxicity in Mice Following AAV Gene Delivery: A Safety Concern for Human Gene Therapy? *Mol Ther*. 2016;24(2):198-201. doi:10.1038/mt.2016.17

20. Kalra A, Yetiskul E, Wehrle CJ, Tuma F. Physiology, Liver. In: *StatPearls*. StatPearls Publishing; 2022. Accessed December 10, 2022. http://www.ncbi.nlm.nih.gov/books/NBK535438/

21. Tso P, McGill J. The Physiology of the Liver. :12.

22. Manco R, Itzkovitz S. Liver zonation. *J Hepatol*. 2021;74(2):466-468. doi:10.1016/j.jhep.2020.09.003

23. Acharya P, Chouhan K, Weiskirchen S, Weiskirchen R. Cellular Mechanisms of Liver Fibrosis. *Front Pharmacol*. 2021;12:671640. doi:10.3389/fphar.2021.671640

24. Westerhoff M, Lamps L. Liver: anatomy, microscopic structure, and cell types. In: Wang TC, Camilleri M, Lebwohl B, et al., eds. *Yamada's Atlas of Gastroenterology*. 1st ed. Wiley; 2022:59-68. doi:10.1002/9781119600527.ch8

25. Piccolo P, Rossi A, Brunetti-Pierri N. Liver-directed gene-based therapies for inborn errors of metabolism. *Expert Opin Biol Ther*. 2021;21(2):229-240. doi:10.1080/14712598.2020.1817375

26. Kisseleva T, Brenner D. Molecular and cellular mechanisms of liver fibrosis and its regression. *Nat Rev Gastroenterol Hepatol*. 2021;18(3):151-166. doi:10.1038/s41575-020-00372-7

27. Kim YO, Popov Y, Schuppan D. Optimized Mouse Models for Liver Fibrosis. In: Clausen BE, Laman JD, eds. *Inflammation*. Vol 1559. Methods in Molecular

Biology. Springer New York; 2017:279-296. doi:10.1007/978-1-4939-6786-5_19

28. Oishi K, Arnon R, Wasserstein MP, Diaz GA. Liver transplantation for pediatric inherited metabolic disorders: Considerations for indications, complications, and perioperative management. *Pediatr Transplant*. 2016;20(6):756-769. doi:10.1111/petr.12741

29. Buiakova OI, Xu J, Lutsenko S, et al. Null Mutation of the Murine ATP7B (Wilson Disease) Gene Results in Intracellular Copper Accumulation and Late-Onset Hepatic Nodular Transformation. *Hum Mol Genet*. 1999;8(9):1665-1671. doi:10.1093/hmg/8.9.1665

30. Huster D, Finegold MJ, Morgan CT, et al. Consequences of Copper Accumulation in the Livers of the Atp7b−/− (Wilson Disease Gene) Knockout Mice. *Am J Pathol*. 2006;168(2):423-434. doi:10.2353/ajpath.2006.050312

31. Mauad TH, van Nieuwkerk CM, Dingemans KP, et al. Mice with homozygous disruption of the mdr2 P-glycoprotein gene. A novel animal model for studies of nonsuppurative inflammatory cholangitis and hepatocarcinogenesis. *Am J Pathol*. 1994;145(5):1237-1245.

32. Fickert P, Zollner G, Fuchsbichler A, et al. Ursodeoxycholic acid aggravates bile infarcts in bile duct–ligated and Mdr2 knockout mice via disruption of cholangioles. *Gastroenterology*. 2002;123(4):1238-1251. doi:10.1053/gast.2002.35948

33. Ikenaga N, Liu SB, Sverdlov DY, et al. A New Mdr2−/− Mouse Model of Sclerosing Cholangitis with Rapid Fibrosis Progression, Early-Onset Portal Hypertension, and Liver Cancer. *Am J Pathol*. 2015;185(2):325-334. doi:10.1016/j.ajpath.2014.10.013

34. Maestro S, Weber ND, Zabaleta N, Aldabe R, Gonzalez-Aseguinolaza G. Novel vectors and approaches for gene therapy in liver diseases. *JHEP Rep*. 2021;3(4):100300. doi:10.1016/j.jhepr.2021.100300

35. Blair HA. Valoctocogene Roxaparvovec: First Approval. *Drugs*. 2022;82(14):1505-1510. doi:10.1007/s40265-022-01788-y

36. Tanne JH. FDA approves $3.5m gene therapy for adults with haemophilia B. *BMJ*. Published online November 25, 2022:o2858. doi:10.1136/bmj.o2858

37. Gao G, Vandenberghe LH, Alvira MR, et al. Clades of Adeno-Associated Viruses Are Widely Disseminated in Human Tissues. *J Virol*. 2004;78(12):6381-6388. doi:10.1128/JVI.78.12.6381-6388.2004

38. Flotte TR, Berns KI. Adeno-Associated Virus: A Ubiquitous Commensal of Mammals. *Hum Gene Ther*. 2005;16(4):401-407. doi:10.1089/hum.2005.16.401

39. Zincarelli C, Soltys S, Rengo G, Rabinowitz JE. Analysis of AAV Serotypes 1–9 Mediated Gene Expression and Tropism in Mice After Systemic Injection. *Mol Ther*. 2008;16(6):1073-1080. doi:10.1038/mt.2008.76

40. Li S, Ling C, Zhong L, et al. Efficient and Targeted Transduction of Nonhuman Primate Liver With Systemically Delivered Optimized AAV3B Vectors. *Mol Ther*. 2015;23(12):1867-1876. doi:10.1038/mt.2015.174

41. Wang L. Comparative Study of Liver Gene Transfer With AAV Vectors Based on Natural and Engineered AAV Capsids. *Cell Ther*. 2015;23(12):11.

42. Vercauteren K, Hoffman BE, Zolotukhin I, et al. Superior In vivo Transduction of Human Hepatocytes Using Engineered AAV3 Capsid. *Mol Ther*. 2016;24(6):1042-1049. doi:10.1038/mt.2016.61

43. Salganik M, Hirsch ML, Samulski RJ. Adeno-associated Virus as a Mammalian DNA Vector. Chandler M, Craig N, eds. *Microbiol Spectr*. 2015;3(4):3.4.04. doi:10.1128/microbiolspec.MDNA3-0052-2014

44. Akache B, Grimm D, Pandey K, Yant SR, Xu H, Kay MA. The 37/67-Kilodalton Laminin Receptor Is a Receptor for Adeno-Associated Virus Serotypes 8, 2, 3, and 9. *J Virol*. 2006;80(19):9831-9836. doi:10.1128/JVI.00878-06

45. Lee EJ, Guenther CM, Suh J. Adeno-associated virus (AAV) vectors: Rational design strategies for capsid engineering. *Curr Opin Biomed Eng*. 2018;7:58-63. doi:10.1016/j.cobme.2018.09.004

46. Chowdary P, Shapiro S, Makris M, et al. Phase 1–2 Trial of AAVS3 Gene Therapy in Patients with Hemophilia B. *N Engl J Med*. 2022;387(3):237-247. doi:10.1056/NEJMoa2119913

47. Jeyakumar JM, Kia A, Tam LCS, et al. Preclinical evaluation of FLT190, a liver-directed AAV gene therapy for Fabry disease. *Gene Ther*. Published online January 11, 2023. doi:10.1038/s41434-022-00381-y

48. Dane A, McIntosh J, Lee D, et al. Preclinical Evaluation of an Engineered AAV Capsid in Non-Human Primates for the Treatment of Haemophilia B. *Blood*. 2018;132(Supplement 1):2197-2197. doi:10.1182/blood-2018-99-117969

49. Marsic D, Govindasamy L, Currlin S, et al. Vector Design Tour de Force: Integrating Combinatorial and Rational Approaches to Derive Novel Adeno-associated Virus Variants. *Mol Ther*. 2014;22(11):1900-1909. doi:10.1038/mt.2014.139

50. Zinn E, Pacouret S, Khaychuk V, et al. In Silico Reconstruction of the Viral Evolutionary Lineage Yields a Potent Gene Therapy Vector. *Cell Rep*. 2015;12(6):1056-1068. doi:10.1016/j.celrep.2015.07.019

51. Grimm D, Lee JS, Wang L, et al. In Vitro and In Vivo Gene Therapy Vector Evolution via Multispecies Interbreeding and Retargeting of Adeno-Associated Viruses. *J Virol*. 2008;82(12):5887-5911. doi:10.1128/JVI.00254-08

52. Lisowski L, Dane AP, Chu K, et al. Selection and evaluation of clinically relevant AAV variants in a xenograft liver model. *Nature*. 2014;506(7488):382-386. doi:10.1038/nature12875

53. Greuter T, Shah VH. Hepatic sinusoids in liver injury, inflammation, and fibrosis: new pathophysiological insights. *J Gastroenterol*. 2016;51(6):511-519. doi:10.1007/s00535-016-1190-4

54. Rogers GL, Shirley JL, Zolotukhin I, et al. Plasmacytoid and conventional dendritic cells cooperate in crosspriming AAV capsid-specific CD8+ T cells. *Blood*. 2017;129(24):3184-3195. doi:10.1182/blood-2016-11-751040

55. van Dijk R, Montenegro-Miranda P, Riviere C, et al. Polyinosinic acid blocks adeno-associated virus macrophage endocytosis in vitro and enhances adeno-associated virus liver directed gene therapy in vivo. *Hum Gene Ther Methods*. Published online August 15, 2013:130815223935004. doi:10.1089/hgtb.2013.086

56. Xu R, Zhang Z, Wang FS. Liver fibrosis: mechanisms of immune-mediated liver injury. *Cell Mol Immunol*. 2012;9(4):296-301. doi:10.1038/cmi.2011.53

57. Grimm D, Pandey K, Nakai H, Storm TA, Kay MA. Liver Transduction with Recombinant Adeno-Associated Virus Is Primarily Restricted by Capsid Serotype Not Vector Genotype. *J Virol*. 2006;80(1):426-439. doi:10.1128/JVI.80.1.426-439.2006

58. Garcia-Bañuelos J, Siller-Lopez F, Miranda A, Aguilar LK, Aguilar-Cordova E, Armendariz-Borunda J. Cirrhotic rat livers with extensive fibrosis can be safely transduced with clinical-grade adenoviral vectors. Evidence of cirrhosis reversion. *Gene Ther*. 2002;9(2):127-134. doi:10.1038/sj.gt.3301647

59. Sobrevals L, Enguita M, Rodriguez C, et al. AAV vectors transduce hepatocytes in vivo as efficiently in cirrhotic as in healthy rat livers. *Gene Ther*. 2012;19(4):411-417. doi:10.1038/gt.2011.119

60. Pañeda A, Vanrell L, Mauleon I, et al. Effect of Adeno-Associated Virus Serotype and Genomic Structure on Liver Transduction and Biodistribution in Mice of Both Genders. *Hum Gene Ther*. 2009;20(8):908-917. doi:10.1089/hum.2009.031

61. Siew SM, Cunningham SC, Zhu E, et al. Prevention of Cholestatic Liver Disease and Reduced Tumorigenicity in a Murine Model of PFIC Type 3 Using Hybrid AAV- *piggyBac* Gene Therapy. *Hepatology*. 2019;70(6):2047-2061. doi:10.1002/hep.30773

62. Murillo O, Luqui DM, Gazquez C, et al. Long-term metabolic correction of Wilson's disease in a murine model by gene therapy. *J Hepatol*. 2016;64(2):419-426. doi:10.1016/j.jhep.2015.09.014

63. Tsui TY, Lau CK, Ma J, et al. rAAV-mediated stable expression of heme oxygenase-1 in stellate cells: A new approach to attenuate liver fibrosis in rats. *Hepatology*. 2005;42(2):335-342. doi:10.1002/hep.20803

64. Paulk NK, Pekrun K, Zhu E, et al. Bioengineered AAV Capsids with Combined High Human Liver Transduction In Vivo and Unique Humoral Seroreactivity. *Mol Ther*. 2018;26(1):289-303. doi:10.1016/j.ymthe.2017.09.021

65. Pekrun K, De Alencastro G, Luo QJ, et al. Using a barcoded AAV capsid library to select for clinically relevant gene therapy vectors. *JCI Insight*. 2019;4(22):e131610. doi:10.1172/jci.insight.131610

66. Cabanes-Creus M, Ginn SL, Amaya AK, et al. Codon-Optimization of Wild-Type Adeno-Associated Virus Capsid Sequences Enhances DNA Family

Shuffling while Conserving Functionality. *Mol Ther - Methods Clin Dev*. 2019;12:71-84. doi:10.1016/j.omtm.2018.10.016

67. Herrmann AK, Bender C, Kienle E, et al. A Robust and All-Inclusive Pipeline for Shuffling of Adeno-Associated Viruses. *ACS Synth Biol*. 2019;8(1):194-206. doi:10.1021/acssynbio.8b00373

68. Huster D. Structural and metabolic changes in *Atp7b* $^{-/-}$ mouse liver and potential for new interventions in Wilson's disease: Copper-induced changes in *Atp7b* $^{-/-}$ mouse liver. *Ann N Y Acad Sci*. 2014;1315(1):37-44. doi:10.1111/nyas.12337

69. Davidoff AM, Ng CYC, Zhou J, Spence Y, Nathwani AC. Sex significantly influences transduction of murine liver by recombinant adeno-associated viral vectors through an androgen-dependent pathway. *Blood*. 2003;102(2):480-488. doi:10.1182/blood-2002-09-2889

70. Rhoads A, Au KF. PacBio Sequencing and Its Applications. *Genomics Proteomics Bioinformatics*. 2015;13(5):278-289. doi:10.1016/j.gpb.2015.08.002

71. Bataller R, Brenner DA. Liver fibrosis. *J Clin Invest*. 2005;115(2):209-218. doi:10.1172/JCI24282

72. Brenner DA. Reversibility of liver fibrosis. *Gastroenterol Hepatol*. 2013;9(11):737-739.

73. Li L, Duan M, Chen W, et al. The spleen in liver cirrhosis: revisiting an old enemy with novel targets. *J Transl Med*. 2017;15(1):111. doi:10.1186/s12967-017-1214-8

74. Kraal G. Cells in the Marginal Zone of the Spleen. In: *International Review of Cytology*. Vol 132. Elsevier; 1992:31-74. doi:10.1016/S0074-7696(08)62453-5

75. Ho WI, Hu Y, Cheng CW, et al. Liposome-encapsulated curcumin attenuates HMGB1-mediated hepatic inflammation and fibrosis in a murine model of Wilson's disease. *Biomed Pharmacother*. 2022;152:113197. doi:10.1016/j.biopha.2022.113197

76. Ertl HCJ. Immunogenicity and toxicity of AAV gene therapy. *Front Immunol*. 2022;13:975803. doi:10.3389/fimmu.2022.975803

77. High-dose AAV gene therapy deaths. *Nat Biotechnol*. 2020;38(8):910-910. doi:10.1038/s41587-020-0642-9